UNIVERSITY OF MINNESOTA

CRACKING OF ASPHALT CONCRETE AT LOW TEMPERATURES

Joseph Labuz,
and Shongtao Dai,
Civil Engineering

CRACKING OF ASPHALT CONCRETE AT LOW TEMPERATURES

FINAL REPORT

submitted to

Center for Transportation Studies
200 Transportation and Safety Building
University of Minnesota

by

Joseph F. Labuz, Associate Professor
Shongtao Dai, Research Assistant
Department of Civil Engineering
University of Minnesota
October 10, 1994

EXECUTIVE SUMMARY

The objectives of this research are (1) to characterize the fracture resistance of asphalt concrete at low temperatures and (2) to develop a simple test method for laboratory testing. Cracking of asphalt concrete at low temperatures is a major problem in the Upper Midwest. The cold temperatures in the winter months impart a brittle behavior to an otherwise ductile (viscous) material. The formation of cracks in the pavement provides a pathway for the migration of water, which may refreeze and cause more damage.

The conventional three-point-bend (3PB) load configuration is proposed for conducting fracture tests. The entire 3PB fixture is placed in an environmental chamber, where the temperature is controlled and maintained at -18° (0°) and -34°C (-30°F). The experimental apparatus and test procedure are described in detail, and the corresponding formulae are derived. Following linear fracture mechanics, the fracture toughness of a particular asphalt concrete at 10% air voids is about 0.5 MPa-$m^{0.5}$ at both temperatures, although the nonlinear response is more pronounced at -18°C. This means that less energy is needed to initiate a crack at -34°C compared to -18°C. Furthermore, it appears that the toughness of the asphalt concrete is increased with an increase in compactive energy, which is indicated by a decrease in air voids content.

The financial support of oil overcharge funds distributed through the Minnesota Department of Administration is acknowledged, but the authors assume complete responsibility for the contents herein.

TABLE OF CONTENTS

CRACKING OF ASPHALT CONCRETE AT LOW TEMPERATURES

1. *Introduction*

Asphalt concrete is composed of brittle inclusions--aggregate--in a viscous matrix--asphalt cement. At temperatures below 0°C (32°F), however, the ductile asphalt behaves like a brittle solid. As such, the failure mode changes from a time-dependent creep response to essentially a time-independent fracture response. The selection of a failure criterion that can be used to estimate the strength and service life of the pavement with respect to cold-temperature cracking must then be fracture-based. Only recently has the concept of linear elastic fracture mechanics been proposed as a way of describing the failure of asphalt at low temperatures (Dongre et al. 1989).

The principles for understanding crack propagation in brittle materials are derived from linear fracture mechanics (LFM). Basically, LFM shows that the stresses at a crack tip are very high, theoretically infinite. These high stresses must be relieved by inelastic deformations that accompany the process of fracture. If this inelastic region is small compared to the grain size of the material--in the case of asphalt concrete this would be the aggregate--and to the dimensions of the structure, then a single parameter called the fracture toughness, K_{Ic}, characterizes the material's resistance to fracture. By knowing K_{Ic}, a stress analysis could be performed to determine if a crack will grow under a given mechanical or thermal loading condition.

Closed-loop, computer-controlled fracture tests were conducted using an unload-reload procedure so that multiple measurements of K_{Ic} may be obtained from a single specimen. Test control and data acquisition was provided by a DEC microcomputer based within an MTS Systems (Minneapolis, MN) servo-hydraulic testing machine. As with any bend test, an accurate measurement of the load-point displacement is complicated by nonlinear deformation and crushing at the roller to specimen contacts. These factors were eliminated by measuring a differential displacement: the deflection of the notch relative to points directly above the supports provides a displacement of the load point that avoids the contact problem. Furthermore, a core-based geometry is proposed as an alternative to the beam with a rectangular cross-section. The cylindrical shape has the advantage that samples may be obtained directly from an existing pavement.

2. *Background*

One of the problems encountered in studying the behavior of flexible pavements is cracking at low temperatures. It is true that some cracking is caused by wear or existing cracks in a stiff base, but some are due to the characteristics of the asphalt itself. Immediately after forming, these cracks have almost no effect on ride quality. However, cracks may lead to other problems such as potholes, spalling, and bumps, and can become a major concern due to their impact on the life of the pavement. This section looks at past studies on bituminous mixtures and the effects of low temperatures, and presents a brief review of fracture mechanics.

2.1 *Asphalt Concrete*

Present design practice of bituminous pavements considers the physical properties of the end product at high temperatures. The mixture must have a certain minimum stability at the maximum expected service temperature of about 60°C. In general, the design restrictions in relation to the range of environmental conditions likely to be experienced by the pavement relate to such things as skid resistance and deformation at the surface. These become less of a problem at lower temperatures and so design in that direction was thought to be unnecessary (Haas and Topper 1969). Another problem with current design is that it is highly empirical. The use of new materials and increased traffic requirements may invalidate some of these empirical criteria.

Initial and final states of damage should be considered when looking at cracking within the pavements. The initial state of damage can be represented by the surface defects, internal flaws, and statistically varying microcracks within the pavement. In testing, this might be lumped into one material constant called the "starter flaw" c_o. The final state is usually defined by one of the cracks meeting or exceeding the critical dimensions and patterns. When the material reaches instability and fails, the crack has reached its critical length c_f (Majidzeh et al. 1971).

Thermal cracking is a significant form of distresses in flexible pavements. It generally manifests itself by transverse cracking at the pavement surface. As the temperature of the pavement surface cools, the surface temperature is lower than that below the surface. This means a temperature gradient develops through the depth of the asphalt concrete (AC) layer because

time is required to conduct the cold into the layer. The surface attempts to contract. However, this contraction is restrained by the lower part of the pavement. Tensile stress builds at the surface and continues to increase when the temperature decreases. On the other hand, as the temperature drops at the surface, the material becomes more brittle. The coupled response eventually leads to tensile stress at the surface exceeding the tensile strength of the material, and surface cracking is initialized. The surface crack may propagate through the AC pavement after several temperature cycles. Consequently, water can migrate through the crack into the base and sub-base. This may cause pumping and quickly lead to pavement failure.

Some researchers have assessed the low-temperature response of asphalt pavements. Hass and Topper (1969) suggested a procedure to estimated the thermally induced stresses in asphalt pavement. It showed a nonlinear distribution through the pavement depth. Christison et al. (1972) derived a thermally induced stress formula by considering the AC pavement as a beam. Newcomb (1984) proposed that the thermal induced stress can be treated as having an approximately uniform distribution through the depth of the AC pavement. In terms of prediction of low-temperature cracking, Hass and Phang (1988) suggested a fracture temperature based on strain. They point out that as the temperature decreases, the tensile strain reaches a material failure strain and cracking results. A fracture temperature of about -10°C was obtained. From a stress-based model, Vinson et al. (1990) provided a fracture temperature of -30°C. Recently, the thermal stress restrained specimen was used to simulate pavement conditions, where a fracture temperature of -17°C was obtained (Jung and Vinson 1991).

Studies have shown that the nature of cracking in asphaltic pavements at low temperatures is similar to cracking of concrete pavements. Both seem to crack due to excessive tensile stresses within the pavement caused by contraction of individual components (Rader 1935). As a check for failure during pavement analysis, the thermal stresses calculated within the material can be compared to the material's tensile strength.

Cracking in asphalt generally does not happen suddenly and completely due to its viscoelastic nature. Initial cracking occurs only to a limited depth and increased stresses are required to propagate the crack. Properties of the asphalt and the asphalt concrete are the basic factors for distress in bituminous layers (Alenowicz et al. 1990). Current models of elastic and viscoelastic pavements indicate that the greatest tensile stress and strain occur at the bottom

of the layer (Alenowicz et al. 1990). Field tests of aged pavements show that the asphalt at the surface was up to ten times stiffer than at the bottom.

Temperature conditions are the most important of the external factors affecting bituminous pavement failure. Temperature has a significant influence on (1) development of thermal stresses in the pavements,

(2) changes in the asphalt concrete strength or toughness, and

(3) relaxation of the stresses in asphalt concrete layers.

Properties of the asphaltic binder are the cause of about 90% of all low-temperature pavement cracking in cold climates (Dongre et al. 1989). A transition temperature can be defined as the temperature at which the asphalt concrete exhibits a behavior change from viscoelastic to elastic. The critical temperature, T_{cr}, is the point at which viscous flow stops and tensile stresses build up with decreasing temperature. The temperature of fracture for the mixture is the point where the strain from thermal loading equals the failure strain (Haas and Phang 1988). For hard bitumens, the cracking temperature falls within the range of typical winter ambient temperatures.

Large temperature gradients can have a significant effect on cracking temperature. For rates less than 5°C/hr, there is minimal change. Temperature drops greater than this results in pavement cracking. Deicing salt can cause cracking from thermal shock, as it can cause as much as a 10°C temperature drop in 0.5 hours (Alenowicz et al. 1990).

Thermal fatigue cracking is another major form of distress in asphaltic pavements. An estimate of the range of temperatures for which thermal fatigue cracking occurs is between -7° (20°) and 21°C (70°F). At higher temperatures, thermal stresses cannot be sustained because of the viscoelastic nature of the binder component. At temperatures below this range, it is believed that immediate failure due to low temperature cracking is the dominating distress mode.

In summary, the three primary causes of low temperature cracking are

(1) thermal stresses in the bituminous surface exceeding the tensile strength or fracture toughness of the mixture;

(2) shrinkage and cracking of the sub-grade from freezing and subsequent propagation upward through the bituminous surface; and

(3) thermal stresses plus traffic loads exceeding the mixture's tensile strength or fracture toughness.

Independent of the cause, cracking might be modeled as a two stage process: initial cracking to a limited depth, then the full-depth propagation of

the crack (Haas and Topper 1969). Other researchers state that low temperature cracks may actually occur as very fine cracks or microcracks during the cold weather. Then as warming occurs, these cracks open up and become visually apparent. The problem with this theory is that if microcracks develop in extreme cold, warming would tend to close the cracks instead of opening them. Another explanation of this could be that the crack initially occurs during the cold period again to a limited depth. Propagation is then a result of a stress increase through the layer caused by warming at the surface. The crack can be seen while the pavement is still relatively cool and disappears with full depth warming (Haas and Topper 1969).

Compaction of a mix is an important factor in developing tensile strength at low temperatures, as paving mixtures are by definition a conglomeration of materials with cracks and voids. With all factors except void content held constant, existing data indicate that specimens containing less voids will have a lower fracture temperature than specimens with a higher void content. The coefficient of thermal expansion relates void content to internal stresses. Asphalt mixtures with relatively large coefficients will have greater stresses. Mixes with lower stiffness due to less compaction and greater void content are less susceptible to low temperature cracking (Alenowicz et al. 1990).

The different materials in asphalt concrete have different susceptibility to cracking. This means that material characteristics such as ductility of the binder, viscosity, and voids content in the mix play an important role in controlling fracture. For example (Haas and Phang 1988), mix stiffness can vary widely with temperature and rate of temperature change. A study of mixes from various sites showed fracture temperatures ranging from -21° to -39°C and the modulus ranging from 2 (0.3 x 10^6) to 9 GPa (1.3 x 10^6 psi) .

The current design methods of AASHTO and FAA are mainly empirical, and thermal cracking is not considered. The mechanistic design based on Miner's method only includes fatigue and rutting of the pavement. Lytton et al. (1983) used linear elastic fracture mechanics to develop a computer-based model to predict thermal fatigue cracking. Anderson et al. (1988) showed that this model cannot be used reliably to relate fundamental AC properties to the incidence of thermal cracking. Dongre et al. (1989) pointed out that the shortcoming of existing fracture mechanics-based models is the fracture parameter being determined from statistical means.

2.2 *Fracture Mechanics*

Because fracture mechanics specifically describes the energy required for cracks to initiate, fracture tests differ from conventional strength tests by requiring that the specimen have a well defined crack. A crack in a solid can be stressed in basically three modes, as illustrated in Figure 1. Stresses applied normal to the crack surfaces give rise to the opening mode called mode I fracture. In-plane shear, referred to as mode II or the sliding mode, results from displacement of the crack surfaces parallel to the plane of the crack. The tearing mode or mode III fracture is caused by out-of-plane shear; the crack surface displacements are in the plane and parallel to the crack front. Any loading condition can be described by the superposition of these three modes of fracture. This work concentrates on mode I (tensile) fracture.

The elastic stress field can be calculated in a two dimensional body of arbitrary size and shape in any mode of loading. For the Cartesian coordinate system, the crack tip stress field can be expressed as

$$\sigma_{ij} = \frac{K_I}{(2\pi r)^{1/2}} f_{ij}(\theta) \tag{1}$$

where σ_{ij} are the stresses acting on a material element at a small distance r from the crack tip at an angle θ from the crack plane, and $f_{ij}(\theta)$ are known functions of θ. Note that theoretically the stresses are singular at the crack tip. The term $K_I/\sqrt{2\pi r}$ must have the dimensions of stress, or K_I must have the dimensions of stress times the square root of length. The stress intensity factor K_I is dependent on the specimen geometry and loading. For an infinite plate with crack length 2a loaded by far-field stress σ, the stress intensity factor can be expressed as

$$K_I = \sigma\ (\pi a)^{1/2} \tag{2}$$

It is assumed that the fracture will extend when K_I reaches a critical value. The critical stress intensity factor or fracture toughness K_{Ic} is the parameter that defines the growth of a fracture. When $K_I > K_{Ic}$, the fracture initiates and propagates in an unstable manner until K_I is less then K_{Ic}. Fracture mechanics may provide a method to establish, in quantitative terms, the effects that composition, stress path or heat treatment have on the service

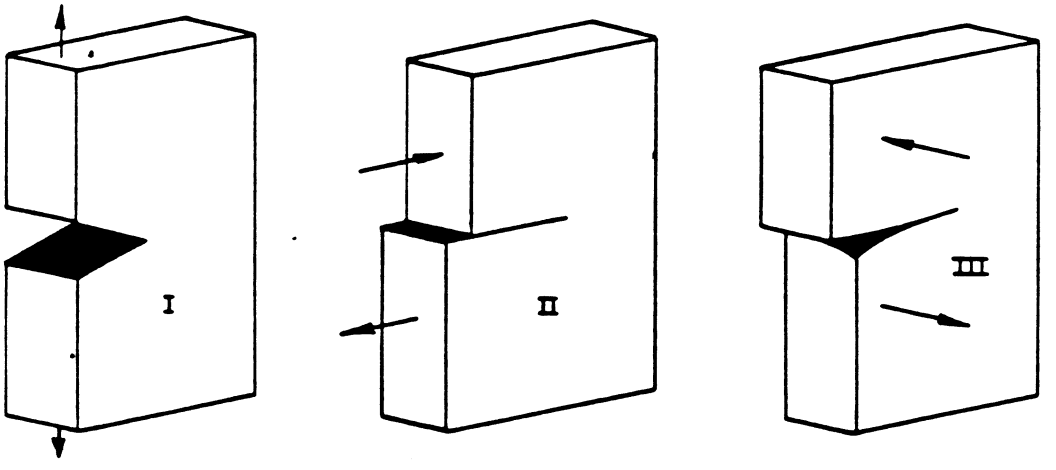

Figure 1. The three modes of fracture.

and performance of asphalt concrete. Fracture testing can be used to determine the suitability of a material for a specific application where the stress conditions are prescribed and where a maximum flaw size (crack length) can be established.

For linear elastic fracture mechanics (LEFM) to apply, the size of the nonlinear region at the crack tip induced by the singular stress field must be negligible in comparison with the crack length and other dimensions of the body. Investigators (Schmidt 1976; Schmidt and Lutz 1979) have shown that linear elasticity is an acceptable assumption for rock-like materials if the scale or specimen size is sufficiently large. Of course, the scale is dependent on the material.

Consider a structure containing a crack that is subjected to mode I loading under controlled displacement conditions; some nonlinear behavior prior to the limit load (point A in Figure 2) may be present due to the severe stress concentration at the crack tip. If the specimen is unloaded and no crack growth occurs during unloading, then the unloading path should be a straight line. In addition, if the crack closes completely such that no permanent or plastic deformation occurs, then the path should return to the origin. This assumption that the crack closes completely and no permanent or plastic deformation occurs is required for strict application of linear fracture mechanics.

If the specimen is displaced to a point further past A, say to C in Figure 2, and produces a crack extension, then energy ΔU is consumed in advancing the crack a distance Δa, where the shaded area OAC is given by

$$\Delta U = \frac{1}{2} F_{avg} \Delta u \tag{3}$$

where F_{avg} is the average load between points A and C and Δu is the load-point displacement between points A and C at the average load. The elastic energy contained in the specimen is represented by the area OAB, but once the crack extends over a length Δa the stiffness of the specimen will decrease to that represented by line OC. Thus, crack propagation from a to $a+\Delta a$ will result in elastic energy release from the specimen equal in magnitude to the area OAC, which may be thought of as the fracture energy. The energy can also include some irrecoverable work (see Figure 3). This may be interpreted as the fracture energy using a nonlinear fracture mechanics approach.

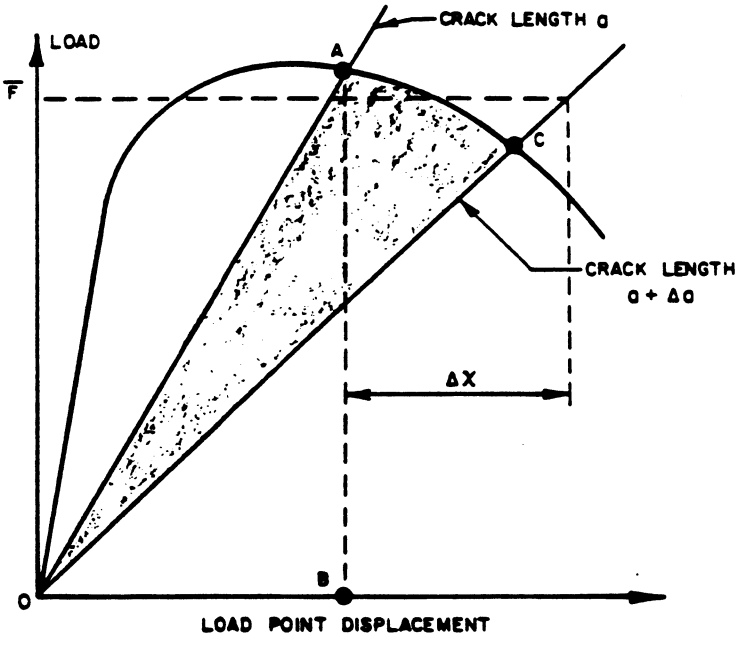

Figure 2. Linear elastic behavior from a fracture test.

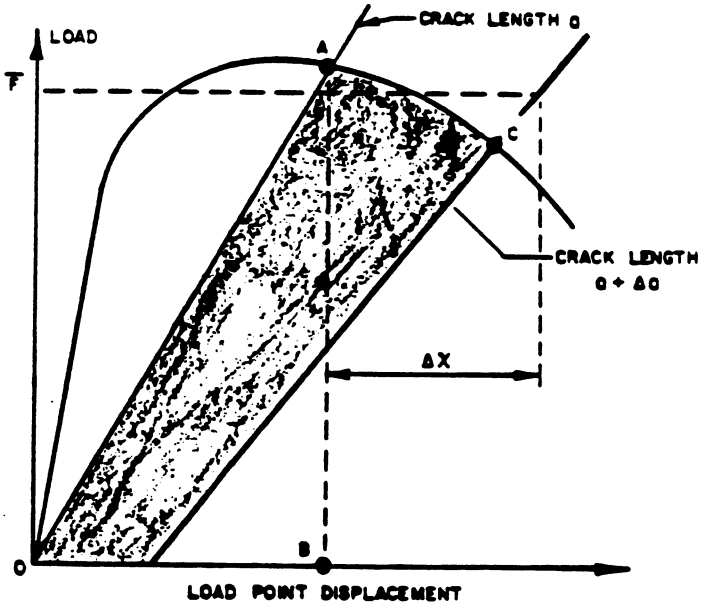

Figure 3. Inelastic behavior from a fracture test.

In experiments for determining fracture toughness, the applied load is directly measured. However, the crack extension Δa is generally microscopic in size, concealed by the sample, or is just difficult to estimate. An indirect measure of crack length was developed by Irwin and Kies (1954) and is known as the compliance method. To apply the compliance method to a given testing geometry and loading configuration, it is important to show that the specimen behaves according to linear elastic fracture mechanics and that the compliance is independent of material properties. Once this has been established the stress intensity factor K_I can be calculated.

The energy release per unit crack extension G_I is given by

$$G_I = \frac{\Delta U}{B\ \Delta a} \tag{4}$$

where B is the specimen thickness. The incremental change in the load-displacement response of the test specimen is known as the compliance λ for a given specimen geometry and loading configuration:

$$\lambda_i = \frac{\Delta u}{F_{avg}} \tag{5}$$

where λ_i is the initial compliance. The tangent of the initial load-displacement slope will provide a value for the initial compliance. A method for obtaining the initial compliance of a specimen is to load the specimen incrementally and plot the load versus load-point displacement. For non-ideal brittle materials such as asphalt concrete, nonlinear processes occur such that some residual displacement of the load point is observed following a load-unload cycle (see Figure 3). So as seen by comparing Figure 2 for an ideal material with Figure 3 for nonideal materials, some corrections may be warranted to adjust for these nonlinearities and hysteresis effects in evaluating fracture toughness of non-ideal materials. Combining equations (3) and (5):

$$\Delta U = \frac{1}{2} F_{avg}^2\ \lambda_i \tag{6}$$

Substituting ΔU from equation (4) and taking the limit as the incremental change in crack length Δa approaches zero yields

$$G_I = \frac{1}{2B} F^2 \frac{d\lambda}{da} \tag{7}$$

where F is the load evaluated at the critical crack length **a**. It can be shown that the energy release rate G_I is related to the stress intensity factor K_I by

$$K_I = [\ \frac{G_I E}{(1-\nu^2)}\ ]^{1/2} \tag{8}$$

where E is Young's modulus and ν is Poisson's ratio.

2.3 *Fracture Toughness Testing of Metals (ASTM E399)*

The validity of a fracture test is dependent on the establishment of a sharp crack at the tip of a notched specimen of adequate size. ASTM E399 "Plane-Strain Fracture Toughness of Metallic Materials" requires that the notched specimen have a minimum thickness of 6.4 mm (0.25 in.) and a well-defined fatigue crack. One suggested specimen is loaded opposite the precracked-single-edged notched beam in three-point bending. To establish a suitable crack-tip condition, the stress intensity level for the fatigue precracking of the specimen is limited to a relatively low cyclic load value. The fracture toughness value is calculated from an equation which has been established on the basis of an elastic stress analysis for the particular geometry and from the load versus load-point displacement record.

According to this method, plane strain fracture toughness is computed at the lowest load at which significant measurable extension of the crack occurs. Significant measurable extension is defined in terms of the load-displacement curve. The load corresponding to a two percent increment of crack extension, which is established as significant measurable extension, is specified by a deviation from the linear portion of the load versus load-point displacement record. In some instances, this may coincide with the maximum load, but frequently the specimen will sustain a higher load than that at which significant crack extension occurs.

The three-point bend fixture should be designed to minimize friction between the specimen and the supports. The frictional effect can be eliminated if the test fixture, while maintaining contact between the specimen and support, allows the support to move or rotate. The support fixture recommended in

ASTM E399 is shown in Figure 4; it can be seen that the support rollers are limited to extensional movement caused by bending of the specimen. A notch displacement gage or clip gage is attached to the specimen to measure the displacement of the notch opening, also known as the crack mouth opening displacement (CMOD).

The specimen geometry is a critical requirement to ensure plane-strain crack extension. The geometry shown in Figure 4 requires that the crack length be nominally equal to the thickness, and be between 0.45 and 0.55 times the depth (W). The fatigue crack is to be extended from the notch and must be greater than five percent of the notch length. To determine when this requirement is met it is usually sufficient to observe the traces of the crack on the outside surfaces of the specimen. A complete measurement of the specimen's initial geometry is required for evaluation of the fracture toughness. Once the specimen is set into the support fixture and the clip gage installed, it is then loaded at a rate that will minimize the effects of stress corrosion.

The notch configuration can consist of the straight edge or the chevron type. Figure 5 shows the requirements of geometry for the chevron starter notch. The chevron notch forces the cracking to initiate at the center of the specimen thickness and thereby increases the probability of a symmetric crack front. This then eliminates the requirement of a fatigue crack as required in the fracture testing of straight notched metal samples. It also helps in providing a "guide" for the crack edges to follow. An additional advantage of the chevron notch is that the fatigue crack will start almost immediately upon cycling and will induce a uniform tensile crack to start at the notch tip. Since the nonsingular stress distribution ahead of the crack is a function of the stress distribution in the uncracked specimen, it is expected that the process zone will only dominate for small cracks.

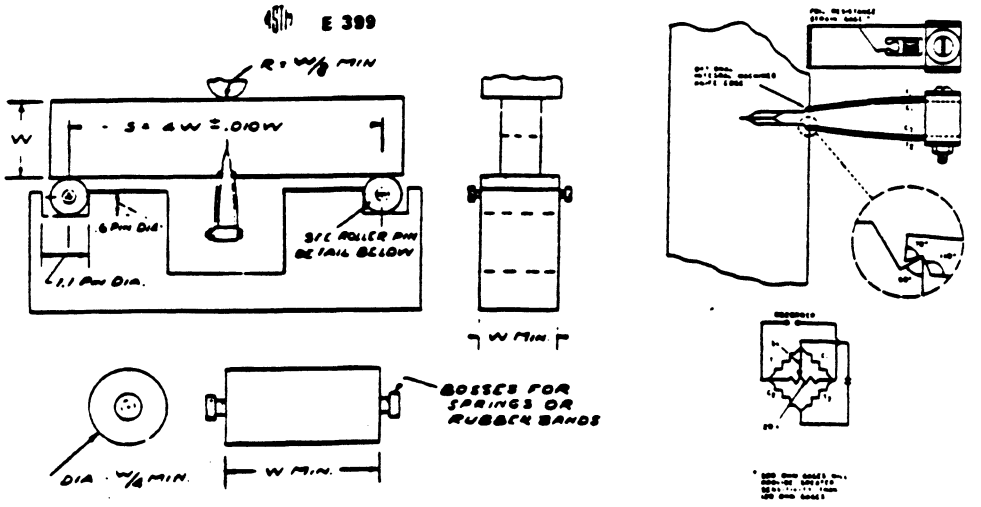

Figure 4. 3PB fixture for toughness testing of metals (ASTM E399).

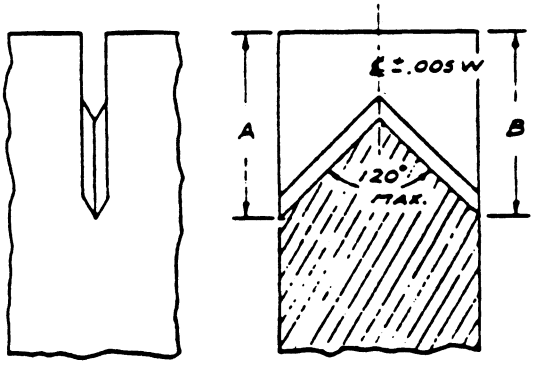

Figure 5. Chevron starter notch for metals (ASTM E399).

3. *Experimental Procedure for Fracture Testing*

The asphalt concrete used for this study is a standard MNDOT mix, type 2341, asphalt grade of 85/100; the air voids content varied between 7% and 14% and was obtained through static compaction with a 1 MN (220 kips) hydraulic load frame. A casting mold 355.6 x 76.2 x 95.25 mm (14 x 3 x 3.75 in.) fabricated from 13 mm (0.5 in.) steel plates was used for all specimen preparation. The desired air voids was achieved by placing the hot (150°C) mix in three lifts, and compressing the asphalt at 450 kN (100 kips) for 60 - 120 s. Figure 6 illustrates the compactive effort vs. air voids. The specimens were allowed to cool at room temperature for about four hours, and were then placed in an environmental chamber where a temperature of 0°C was achieved gradually over a period of four hours. Approximately one day prior to testing, the temperature of the chamber was adjusted to the testing temperature.

A closed-loop, servo-controlled testing machine utilizes a program written for the particular experiment such that the position of the hydraulic actuator is constantly adjusted to follow the command signal. Whether the material is behaving elastically or inelastically, the system attempts to follow the program. A signal from the experiment, generated by the specimen and measured by a transducer, is electronically compared with the program instruction, as illustrated in Figure 7. If an error exists, that is, the transducer feedback is not at the required value as determined by the program, then a servo-valve in the hydraulic system is automatically adjusted until the transducer response coincides with the program. For further information on closed-loop, servo-controlled testing refer to Labuz et al. (1985).

3.1 *Load Apparatus and Instrumentation*

Three-point-bend testing requires that a compressive load be applied to the beam surface opposite the notch. The loading fixture is designed to minimize frictional effects through the use of rollers (as suggested by ASTM E399). The entire support fixture was constructed of stainless steel. The initial roller position is maintained by soft springs and backstops which establish the test span dimension. The support rollers are allowed to rotate out away from the backstops during the test but will remain in contact with the sample. The roller support blocks are secured to a 12.7 mm thick base plate

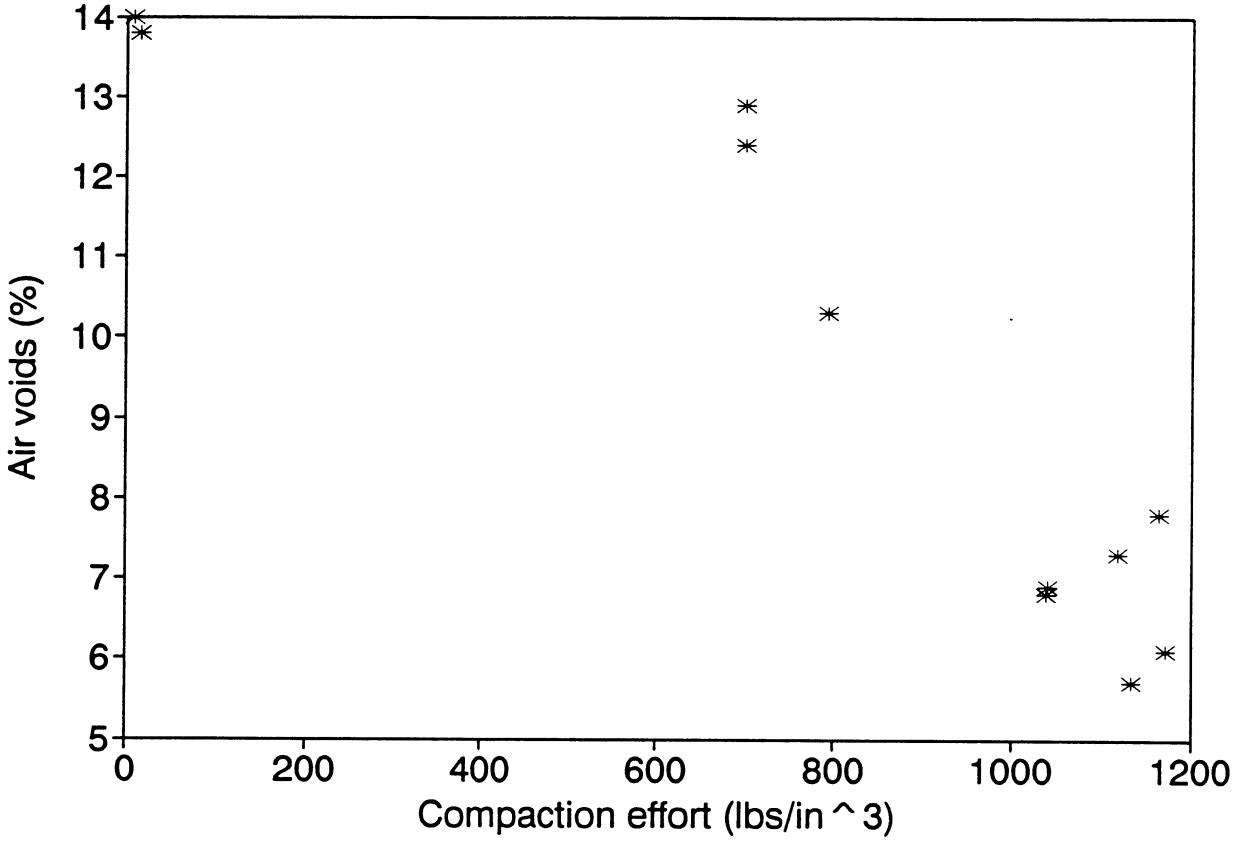

Figure 6. Compactive effort for asphalt concrete specimens.

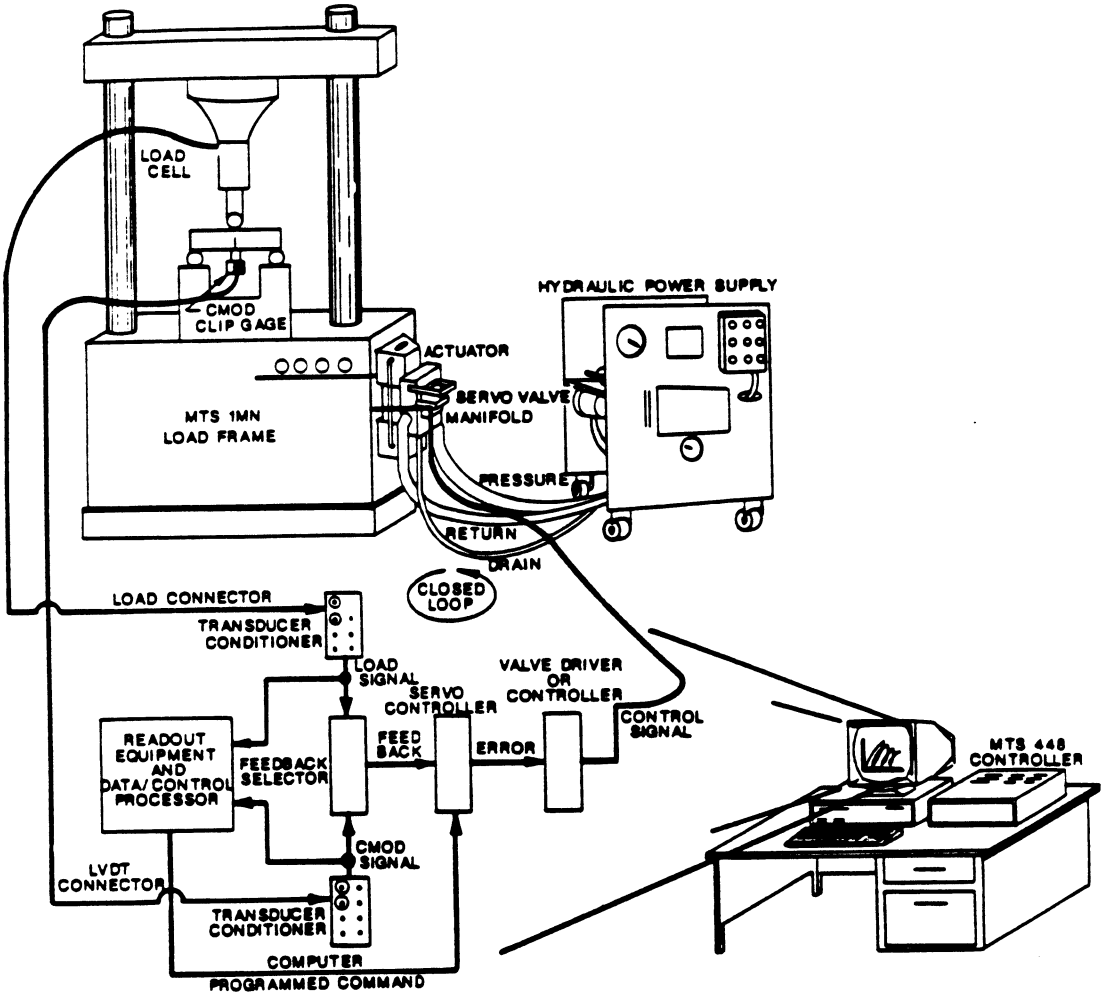

Figure 7. Closed-loop, servo-hydraulic testing system.

with a 9.5 mm diameter dowel hole for alignment with the actuator center. The span dimension is required to be set at 4.0 times the beam height.

To obtain an accurate measure of the load-point displacement (LPD), a reference frame called the saddle (see Figure 8), supported by the sample at the locations opposite the support rollers, was designed. The saddle allows the upper loading roller to pass freely through the plate and provides a location for two linear variable differential transformers (LVDTs) to measure the load-point displacement. The saddle for this work was constructed of a 12.7 mm thick, 209.6 x 133.4 mm stainless steel plate. The roller opening was cut to 1.3 mm larger than the loading roller to allow friction-free movement. The saddle will remain parallel to the original core axis during the loading process (unless crushing of the specimen on the support rollers occurs) with the saddle supported on the specimen by leveling screws directly over the support rollers.

To successfully measure the load-point displacement with the saddle as the reference frame, contact with some portion of the specimen is required. In this design the LVDT platen and yoke shown in Figure 9, makes contact with the notch front. The yoke is made of a thin but stiff piece of stainless steel. Two LVDT platens are secured to the shoulders of the yoke. The two LVDTs measure the displacement of the notch front at two points relative to the saddle. The signal from the two LVDTs is acquired separately but averaged to correct for twisting of the specimen. Special brass LVDT holders shown in Figure were made for the RDP 1000 series LVDTs. The 1.6 mm (1/16 in.) thick brass sleeve is split for flexibility and has a 3.2 mm (1/8 in.) wide collar to butt against the saddle. A set screw is placed within the side of the saddle adjacent to the LVDT to clamp the brass sleeve and LVDT into position.

All transducers (load cell, clip gage and two LVDTs) were calibrated prior to testing. The load cell was a Lebow 22.5 kN cell model-3132; the clip gage, an MTS clip-on gage model 632-02B-20; and the two LVDTs, RDP model-GTX1000. The load cell has a linear range of 22.5 kN (5 kips) and was initially calibrated using dead weights applied directly to the load cell. The load cell was periodically calibrated using a proving ring at room temperature. The clip gage has a linear range of 2.5 mm (0.1 in.) and was calibrated using a Schaevitz 41M calibration micrometer and a clip gage stand. The clip gage and MTS 448.21-R1 conditioner were calibrated to 0.0027 mm/volt (0.01 in./volt) at room temperature and periodically checked with the Schaevitz 41M calibration stand during the testing program. The two RDP LVDTs (s/n 2972 and s/n 2973) have a linear range of 0.25 mm (0.01 in.) and

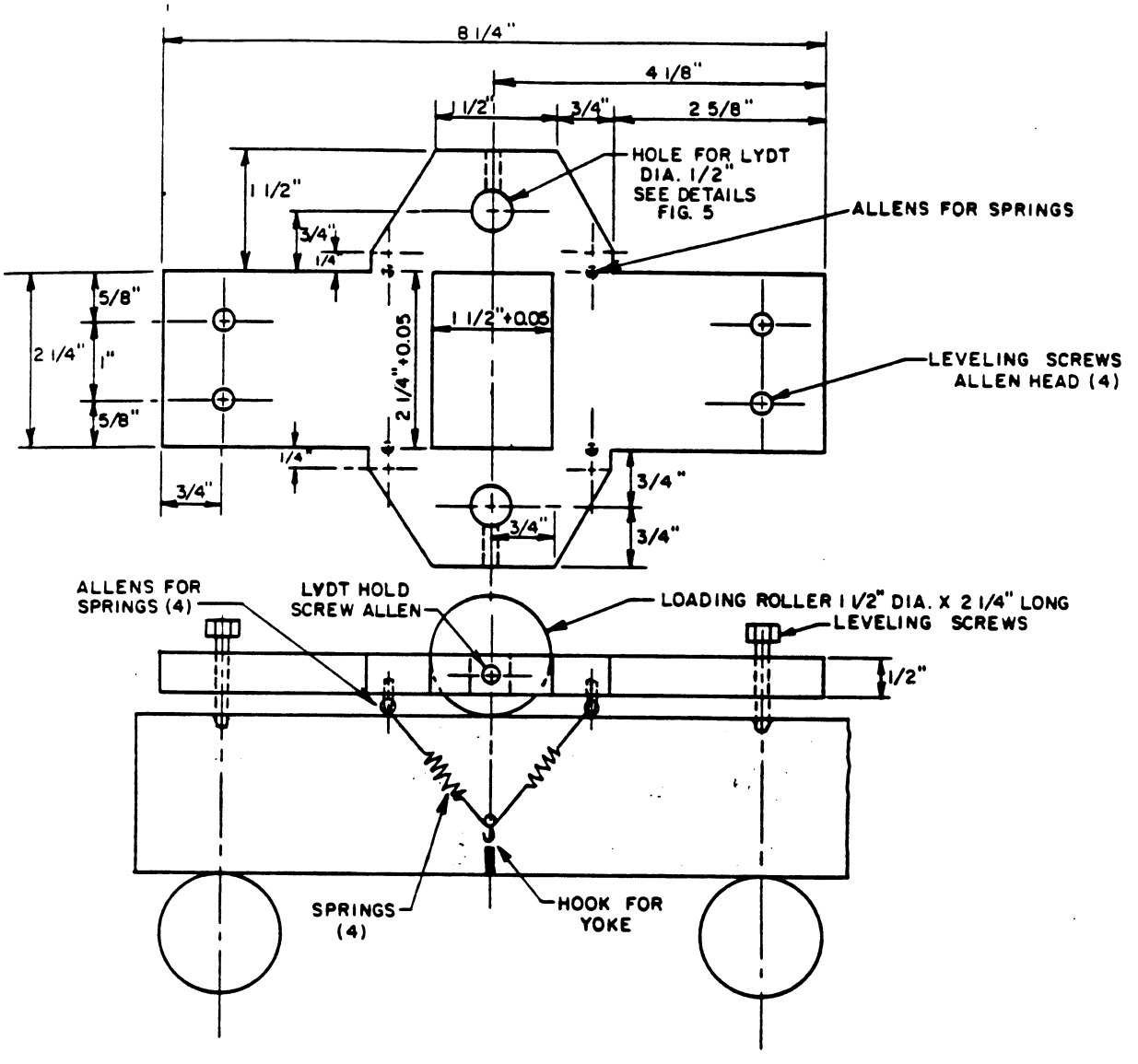

Figure 8. Reference frame for load-point displacement (shown for core specimens).

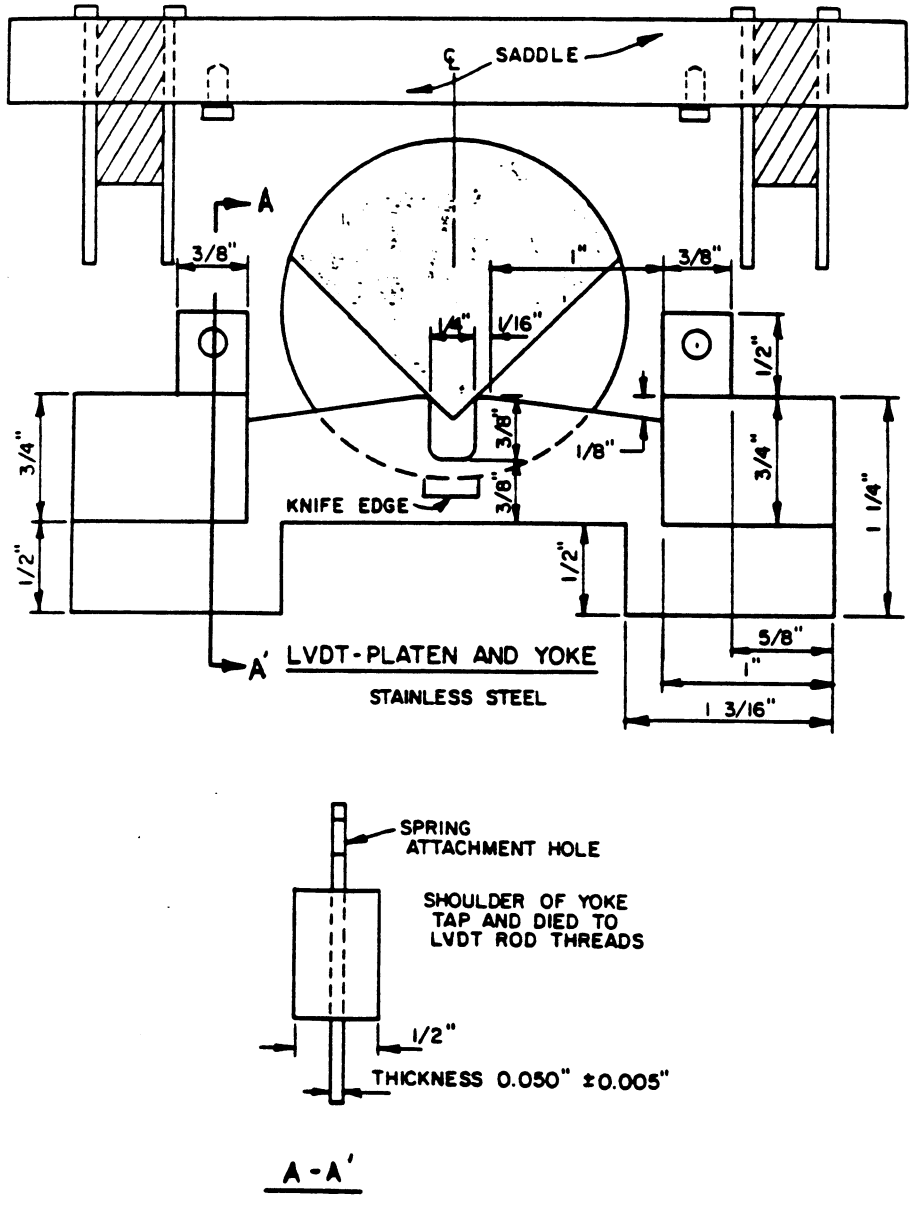

Figure 9. LVDT platen and yoke (shown for core specimens).

were calibrated initially utilizing gage blocks and the "saddle" device to secure the LVDTs. The Schaevitz 41M calibration stand was utilized to periodically check the gage calibration during the testing period. The two LVDTs were calibrated to 1.75E-2 and 1.69E-2 mm/volt (6.88E-4 and 6.65E-4 in./volt) at room temperature. The sensitivity of LVDTs is affected by temperature, so calibration also was performed at the testing temperatures.

An MTS 815 Rock Mechanics Test system with a 448 controller and an MTS 1 MN (220 kips) four column load frame was used. The test system, data acquisition and data reduction was computer-controlled using a PDP 11/73 microcomputer. The testing software (MTS BASIC) was generated to coincide with the spirit of the ASTM suggested method. The software, along with an explanation of the variables used and logic behind the programming generated for this testing, is presented in Appendix 7.1.

3.2 *Compliance Calibration*

The compliance λ is defined as u/F, where u is the load-point displacement and F is the load. In linear elastic fracture mechanics, the compliance is useful in determining the crack length for a given geometry and material. The compliance can be transformed into a dimensionless compliance, $g = \lambda EB$, which essentially is independent of material behavior.

For the three-point-bend test, the dimensionless compliance g can be obtained as a function of the dimensionless crack length $\alpha = a/W$. In this project, a curve of g vs α for an aluminum (2024) specimen was obtained experimentally and compared with the theoretical curve, which can be used to determine the crack length of the asphalt concrete (AC) specimens under the three-point-bend test from the loading record.

Recall that the strain energy release rate (G_I) can be expressed as

$$G_I = \frac{1-\nu^2}{E} K_I^2 \quad (\textit{plane strain}) \tag{9}$$

For the three point bend test, K_I is given as (ASTM E399-90)

$$K_I = \frac{F\,S}{B\,W^{3/2}} f(\alpha) \tag{10}$$

where

$$f(\alpha) = \frac{3\alpha^{1/2}[1.99-\alpha(1-\alpha)(2.15-3.93\alpha+2.7\alpha^2]}{2(1+2\alpha)(1-\alpha)^{3/2}} \tag{11}$$

The total compliance of the specimen is

$$\lambda = \lambda_{NC} + \lambda_C \tag{12}$$

where λ_{NC} is the compliance of the beam without the crack, and λ_C is the compliance due to the crack; λ_{NC} can be found in an elasticity textbook (Sokolnikoff 1956):

$$\lambda_{NC} = [\frac{S^3}{48EI} + \alpha_s\frac{S}{4GA} + \frac{(S+25W)}{5EBW}] \tag{13}$$

where I is the moment of inertia, G is the shear modulus, A is the cross-sectional area, α_s is the shear factor (for rectangle beams $\alpha_s = 1.2$).

To calculate λ_C, the load-point displacement due to the crack can be expressed as

$$u_C = \frac{\partial}{\partial F}\int_0^{aB} G_I \, d\Gamma \tag{14}$$

where $\Gamma = \xi B$, and ξ is the crack length at a certain time. Combining equations (9) and (10), (14) becomes

$$u_C = \frac{2\ (1-\nu^2)FS^2}{EBW^2}\int_0^{\alpha} f(x)\ dx \tag{15}$$

where $x = \xi/W$. So, the compliance due to the crack is

$$\lambda_C = \frac{2\ (1-\nu^2)S^2}{EBW^2}H(\alpha) \tag{16}$$

where

$$H(\alpha)=\int_0^{\alpha} f(x)\,dx = 0.495/(1-\alpha)^2+\frac{0.5853}{(\alpha-1)}-19.38\alpha+8.717\alpha^2-6.098\alpha^3+2.984\alpha^4$$

$$-0.821\alpha^5+\frac{5.194}{(1+2\alpha)}-2.285\ LN(1-\alpha)+13.539\ LN(1+2\alpha)-5.1037 \quad (17)$$

From equation (13) and (16), considering G = E/[2(1+ν)], I = BW^3/12, and A = BW, the total compliance can be represented as

$$\lambda=\frac{S^3}{4BEW^3}+\alpha_s\frac{S(1+\nu)}{2BEW}+\frac{S+25W}{5BEW}+\frac{2(1-\nu^2)S^2}{BEW^2}H(\alpha) \quad (18)$$

The dimensionless compliance is g = λEB, so

$$g=\frac{S^3}{4W^3}+\alpha_s\frac{S(1+\nu)}{2W}+\frac{S+25W}{5W}+\frac{2(1-\nu^2)S^2}{W^2}H(\alpha) \quad (19)$$

An aluminum (2024) specimen with varying α (0.25, 0.3, 0.35, 0.4, 0.425, 0.45, 0.475, 0.5, 0.525, 0.55) was loaded using the three-point-bend fixture. The span is 226.1 mm (8.9 in.), the width is 50.8 mm (2 in.), and the thickness is 25.4 mm (1 in.). Young's modulus is 72.4 GPa (10,500 ksi) and Poisson's ratio is 0.32. The dimensional compliance g can be calculated from the linear part of load-load point displacement record for the various α. Figure 10 shows the results between theory and experiment, which are in good agreement.

Once the expression for the dimensionless compliance g is established, an indirect method to determine Young's modulus E is available. The initial geometry, including notch length, is well known so that g can be calculated. The initial compliance λ_i can be measured from repeated load-unload cycles within the elastic response of the material. The modulus E is then simply g/λB.

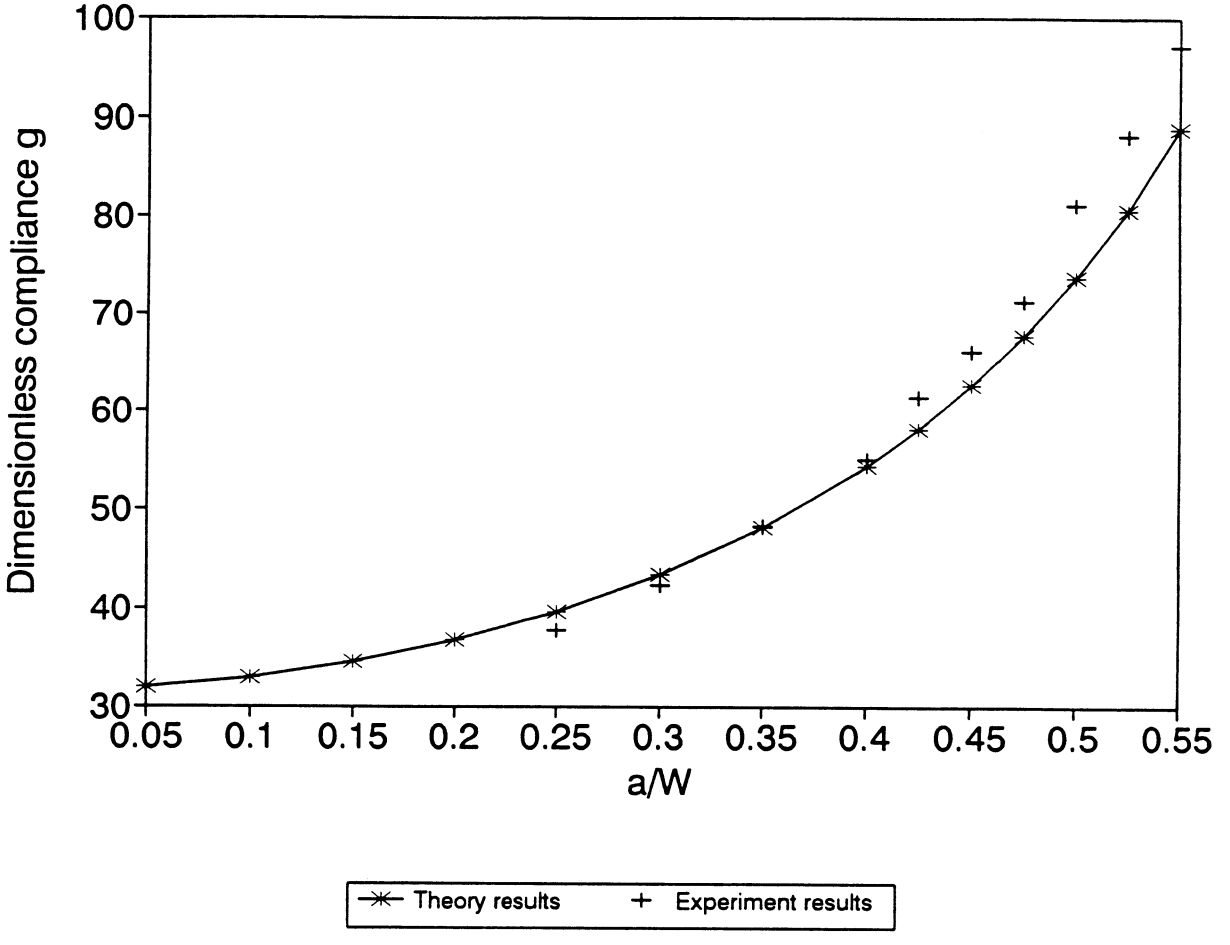

Figure 10. Compliance calibration of the 3PB beam.

4. *Discussion of Results*

The behavior of the asphalt concrete at 0°C was that of either a brittle (Figure 11) or ductile (Figure 12) solid; the difference in behavior is believed to be related to the time the specimen was subjected to the testing temperature prior to failure. For the brittle specimen, the temperature of 0°C was maintained for four hours; K_{Ic} was calculated to be 0.25 MPa-$m^{0.5}$ and E from the beam compliance was 0.4 GPa. For the ductile specimen, the temperature of 0°C was applied for only one hour. A crack was not visible until a displacement (CMOD) of 0.4 mm, an order of magnitude difference in terms of the brittle behavior. In addition, the transition temperature for this asphalt concrete may be around 0°C.

To avoid the inconsistency of the material response near the transition temperature, only the temperatures of -18° and -34°C were considered for fracture testing. A total of twelve specimens were prepared at an air voids content of approximately 10%. Due to experimental difficulties, only seven tests are reported (see Table 1); the load-displacement records are contained in Appendix B. A direct measure of Young's modulus was accomplished by testing the material in uniaxial compression at the designated temperature and measuring the axial displacement. Further work is needed to explain the difference in the two measures of modulus.

Table 1. Experimental results.

Specimen	Temp °C	Peak load kN	K_{Ic} MPa-$m^{0.5}$	E_{beam} GPa	E_{direct} GPa
3	-18	1.30	0.62	9.74	2.24
5	"	1.09	0.47	10.42	2.35
8	"	1.12	0.51	11.44	2.42
9	-34	1.15	0.49	-	-
10	"	1.27	0.54	14.67	6.49
11	"	1.23	0.52	-	4.95
12	"	1.13	0.48	-	5.24

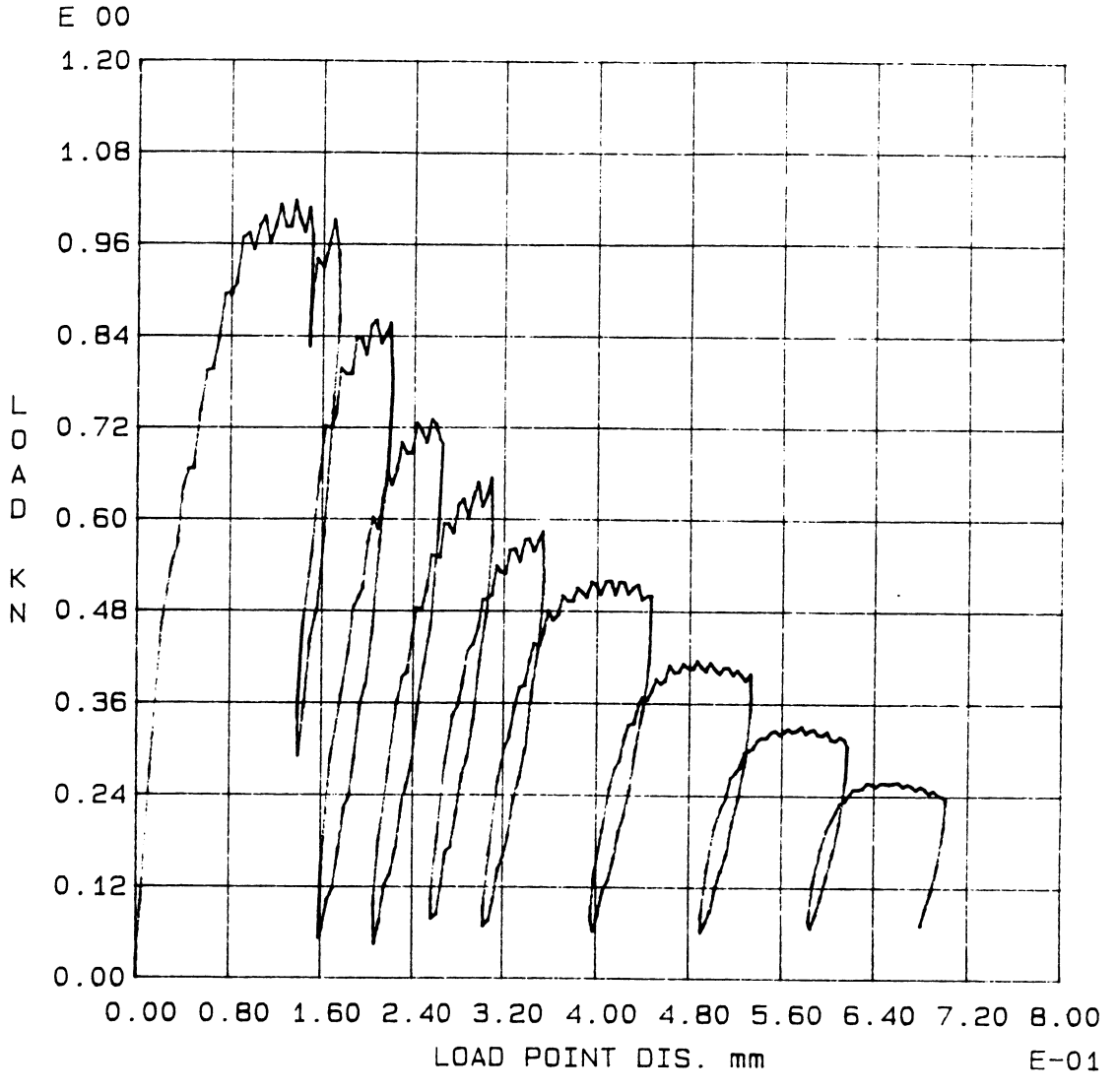

Figure 11. Load record from fracture test at 0°C, with the temperature maintained for 4 hours prior to testing.

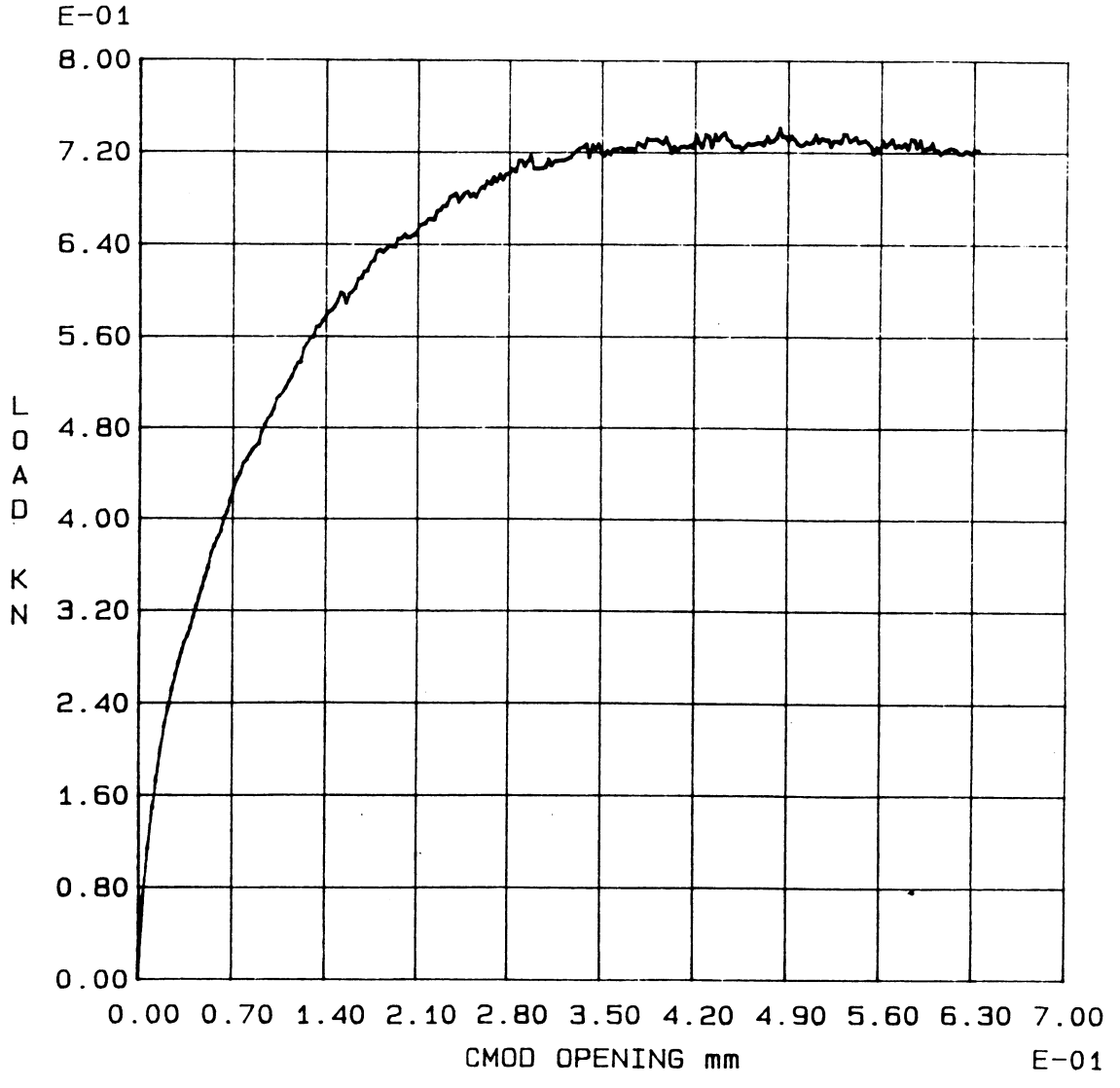

Figure 12. Load record from fracture test at 0°C, with the temperature maintained for 1 hour prior to testing.

Although the data suggest that the fracture toughness of this material is the same at the two temperatures, an examination of the loading records gives a clearer picture (Figures 13 and 14). The geometry, including notch length, was virtually the same for all the specimens, so peak load is directly related to the fracture toughness (the offset method of ASTM was not used to compute K_{Ic}). Substantial nonlinear displacement prior to peak load is evident for the -18°C test, where the load-point displacement (LPD) at peak load is 0.07 mm. The displacement (LPD) at peak for the -34°C test is only 0.035 mm. The increased nonlinear displacement at the higher temperature contributes to the energy consumption in creating new surfaces, but this additional energy is not included in the calculation of K_{Ic}. Further work is needed to quantify this behavior. It can be stated, however, that the energy needed to initiate a fracture is less at -34°C than at -18°C.

By using the closed-loop testing system, crack propagation can be followed after peak load, and multiple measurements of fracture toughness can be determined from the compliance technique. (The specimen is unloaded and reloaded at different stages of displacement; from the slope of the unloading portion the crack length can be estimated.) Table 2 shows the results from the unloading-reloading, and Figure 15 is a plot of the data. An increase in fracture toughness with crack length is apparent, and this behavior is displayed by other brittle materials such as rock (Labuz et al. 1985). The plateau of the curves is probably more representative of the asphalt concrete's resistance to fracture than the initial values because of the inelastic zone at the crack tip.

Fracture mechanics concepts were utilized to assess the resistance of various mixes to the low-temperature cracking by Dongre et al. (1989). They obtained J_{Ic} (a measure of fracture energy including nonlinear behavior) and K_{Ic} at different temperatures and claimed that K_{Ic} is not sensitive to the AC variables. Little and Mahboub (1985) studied the fracture properties of first-generation, plasticized sulfur binders. They recommend using J_{Ic} as a material parameter for sulfur binders. These studies seem to be in agreement with this research, as some correction or continued measurement of fracture toughness is needed.

The influence of compactive energy is demonstrated by two tests performed at -18°C for specimens prepared at two different air voids content--7% and 13%. At the lower air voids (7%), K_{Ic} is 0.7 MPa-$m^{0.5}$, while at the higher air voids, K_{Ic} is 0.2 MPa-$m^{0.5}$.

Table 2. Results from unloading-reloading.

Specimen	Un-re-load Cycle	Crack length, a mm	K_{Ic} MPa-$m^{0.5}$
3	8	21.8	0.52
	9	25.7	0.62
	10	30.8	0.67
5	8	23.4	0.47
	9	23.8	0.45
	10	25.4	0.48
8	8	24.4	0.51
	9	26.9	0.56
	10	28.6	0.61
10	8	23.4	0.54
	9	28.3	0.60
	10	34.6	0.68

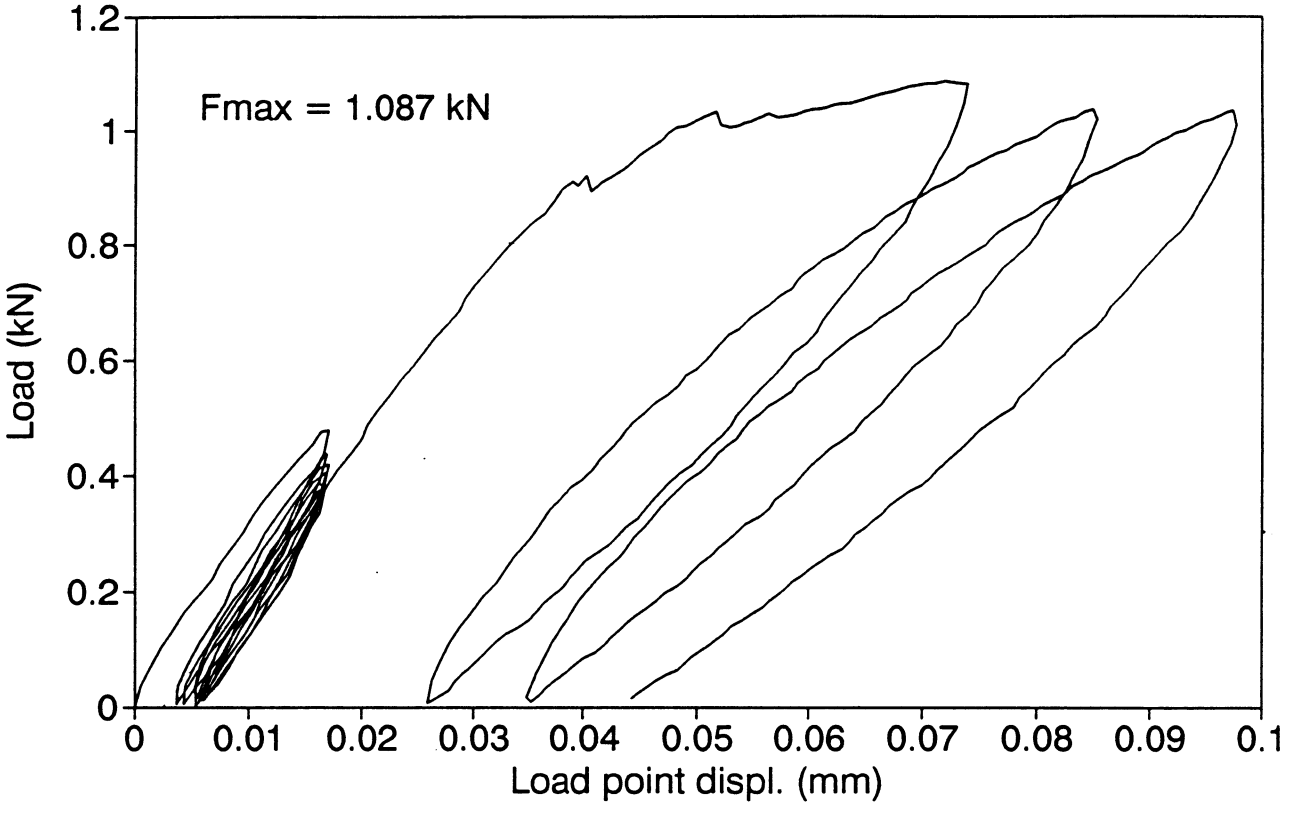

Figure 13. Load record from fracture test at -18°C.

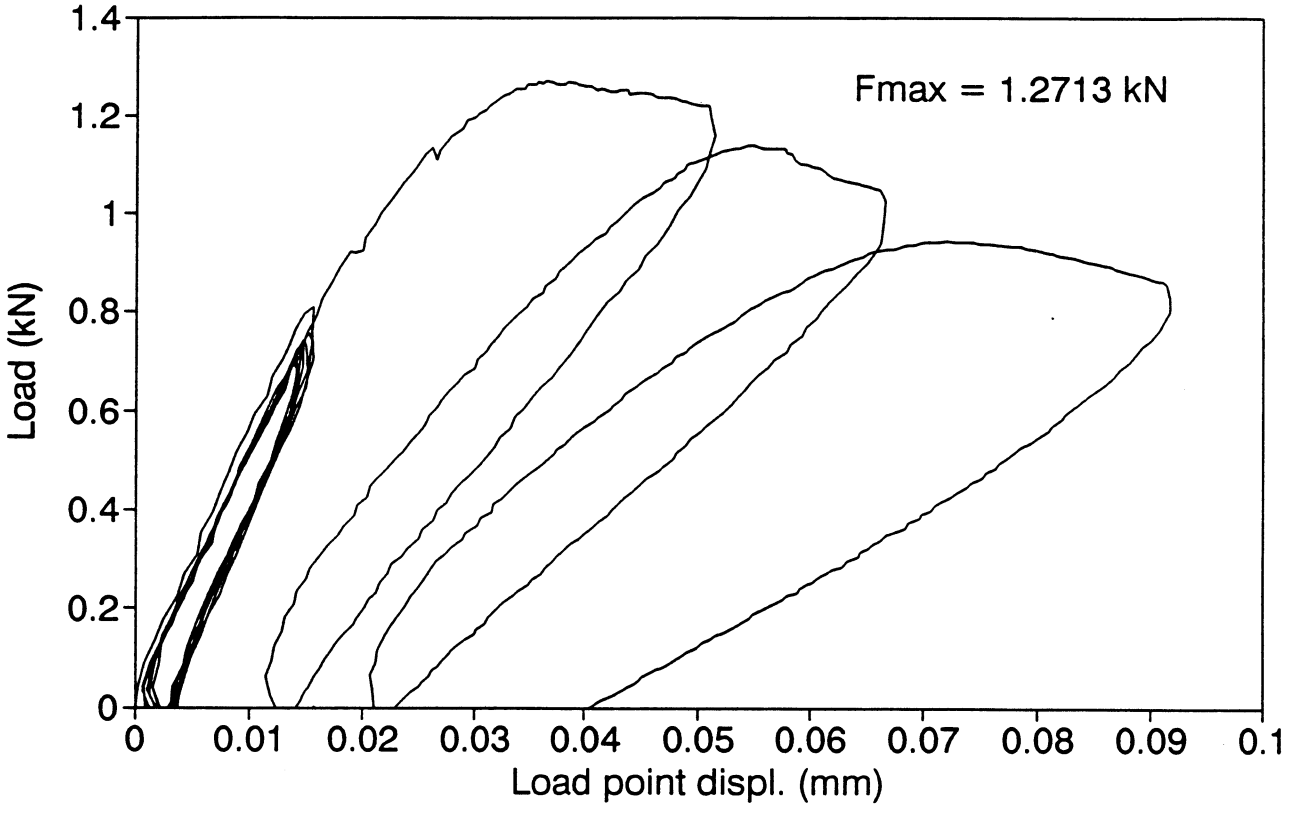

Figure 14. Load record from fracture test at -34°C.

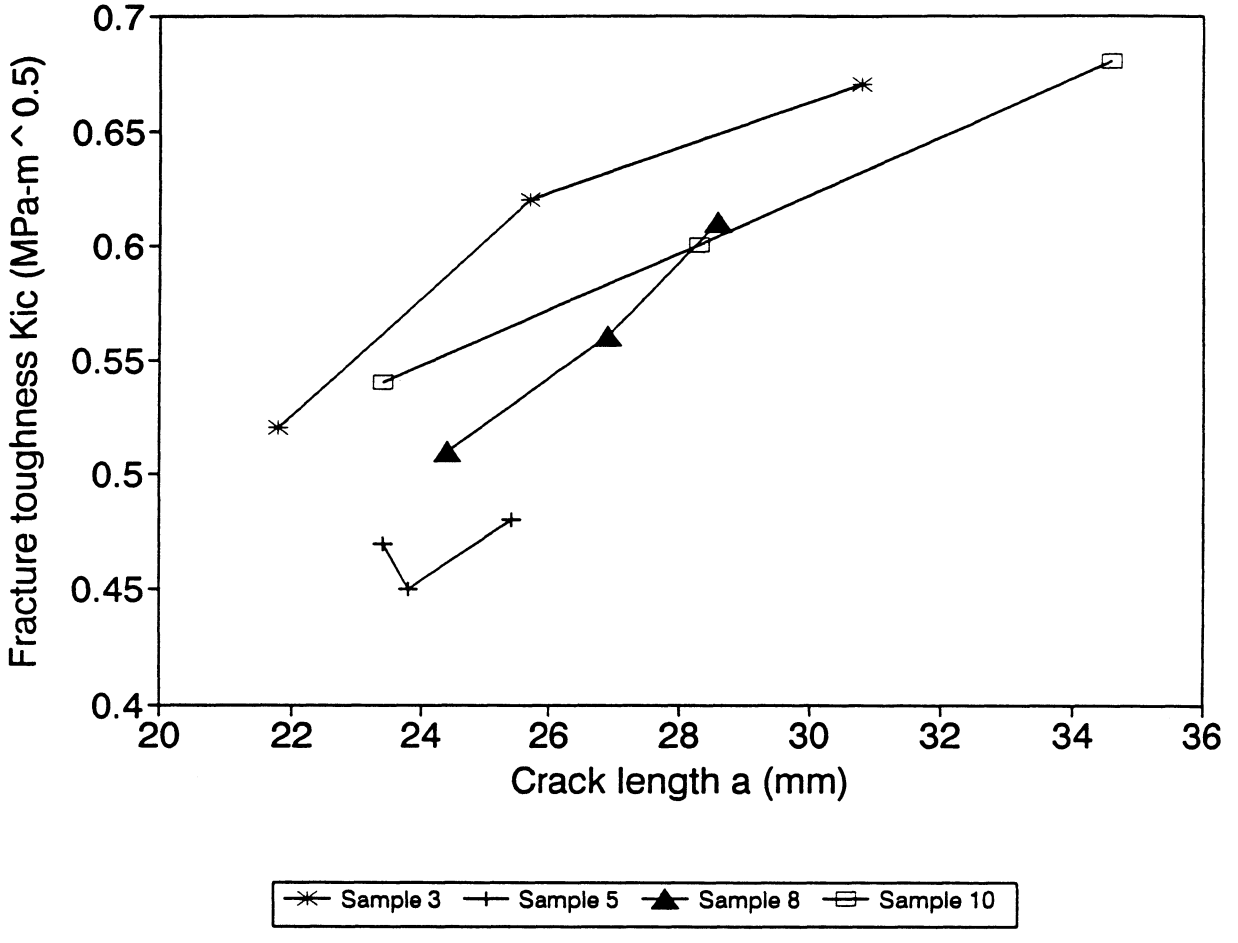

Figure 15. Change in fracture toughness with crack length.

5.1 *Conclusions*

Closed-loop, computer-controlled fracture tests were conducted using an unload-reload procedure so that multiple measurements of fracture toughness K_{Ic} could be obtained from a single specimen in three-point bending. As with any bend test, an accurate measurement of the load-point displacement is complicated by nonlinear deformation and crushing at the roller to specimen contacts. These factors were eliminated by measuring a differential displacement: the deflection of the notch relative to points directly above the supports provides a displacement that avoids the contact problem. This method provides an estimate of Young's modulus E through a compliance calibration.

It appears that the behavior (E and K_{Ic}) of the asphalt concrete tested at an air voids content of about 10% is dependent upon temperature, although the response at 0°C may be near the transition temperature. Assuming linear fracture mechanics is valid, the fracture toughness varied from 0.25 MPa-$m^{0.5}$ at 0° to 0.5 MPa-$m^{0.5}$ at -18° and at -34°C. Nonlinear behavior is more pronounced at -18°, which means that more energy would be needed to initiate the fracture. In terms of pavement performance, this asphalt concrete would be more resistant to cracking at -18° than at -34°C.

Compactive energy influences the asphalt's fracture toughness. For tests conducted at -18°C, specimens prepared at a lower air voids (7%) exhibited K_{Ic} of 0.7 MPa-$m^{0.5}$, while at higher air voids K_{Ic} was 0.2 MPa-$m^{0.5}$.

5.2 *Recommendations*

Fatigue-type loading should be examined in relation to the material's fracture toughness. Typical traffic loads could be simulated in the fracture test at low temperatures, and the performance of the material in terms of crack growth and load cycle could be monitored by a change in compliance.

Furthermore, a core-based geometry is proposed as an alternative to the beam with a rectangular cross-section. The cylindrical shape has the advantage that samples may be obtained directly from an existing pavement.

6. *References*

Alenowicz, J., Kekalainen, R., and Ehrola, E. (1990) Minimizing reflection and frost heave cracking in flexible and semi-rigid road pavements. University of Finland, Publications of Road and Traffic Laboratory.

Anderson, D.A, Christensen, D.W, Dongre, R., Runt, J., and Jordhal, P. (1988) Asphalt behavior at low service temperatures. Final Report FHWA PTI 8802. Pennsylvania Transportation Institute, University Park.

ASTM E399 (1990) Standard test method for plane-strain fracture toughness of metallic material, Annual Book of ASTM Standards, Designation E399-90. Am. Soc. Testing Materials, Philadelphia, pp. 666-681.

Christison, J.T, Murray, D.W, and Anderson, K.O. (1972) Stress predication and low temperature fracture susceptibility. Proceedings Association of Asphalt Paving Technologists, Vol. 41, pp. 494-523.

Dongre, R., Sharma, M.G., and Anderson, D.A. (1989) Development of fracture criterion for asphalt mixes at low temperatures. Transportation Research Record 1228, pp 94-105.

Haas, R.C.G., and Topper, T.H. (1969) Thermal fracture phenomena in bituminous surfaces. National Research Council, Highway Research Board Special Report 101, Washington D.C.

Haas, R.C.G., and Phang, W.A. (1988) Relationships between mix characteristics and low-temperature pavement cracking. Proc AAPT, pp. 290 - 319.

Irwin, G.R., and Kies, J.A. (1954) Critical energy rate analysis of fracture strength, Welding Research Supplement 19, pp. 193-198.

Jung, D. H., and Vinson. T. S. (1991) Interim report on laboratory evaluation of low temperature cracking from thermal stress restrained specimen test. Strategic Highway Research Program. National Research Council, Washington, D.C.

Labuz, J.F., Shah, S.P., and Dowding, C.H. (1985) Experimental analysis of crack propagation in granite. Int. J. Rock Mech. Min. Sci., Vol. 22(2), pp. 85-98.

Little, D.N., and Mahboub, K. (1985) Engineering properties of first generation plasticized sulfur binders and low temperature fracture evaluation of plasticized sulfur paving mixtures. Transportation Research Record 1034, pp. 103-111.

Lytton, R.L., Shanmugham, U., and Garret, B.D. (1983) Design of flexible pavements for thermal fatigue cracking. Report FHWA/TX-83/06+284-4. Texas Transportation Institute.

Mahboub, K. (1990) Elasto-plastic fracture characterization of paving materials at low temperatures. J. Testing Eval. 18(3), pp 210-218.

Majidzdeh, K., Kauffmann, E.M., and Ramsamooj, D.V. (1971) Application of fracture mechanics in the analysis of pavement fatigue. Proc AAPT, Vol. 40, pp. 227-246.

Newcomb, D. (1984) Class notes.

Rader, L.F. (1935) Investigations of the physical properties of asphaltic mixtures at low temperatures. Proc ASTM, Part II, Vol. 35.

Schmidt, R.A. (1976) Fracture toughness testing of limestone. Exp. Mech. 16, pp. 161-167.

Schmidt, R.A. and Lutz, T.J. (1979) K_{Ic} and J_{Ic} of Westerly granite--effects of thickness and in-plane dimensions. Fracture mechanics applied to brittle materials. ASTM STP 678, pp. 166-182.

Sokolnikoff, I.S. (1956) Theory of elasticity, McGraw-Hill.

Vinson, T.S., Janoo, V.C., and Hass, R.C.G. (1990) Summary report - low temperature and thermal fatigue cracking. Report SHRP-A/IR-90-001. Strategic Highway Research Program.

7. *Appendices*

Table A1. Specimen dimensions

Sample	Size (mm)	a_0 (mm)
3	355.6 x 63.5 x 58.2	21.8
5	355.6 x 63.5 x 58.7	23.4
8	355.6 x 63.5 x 57.9	24.4
9	355.6 x 63.5 x 58.7	23.4
10	355.6 x 63.5 x 58.7	23.4
11	355.6 x 63.5 x 58.7	23.1
12	355.6 x 63.5 x 58.7	23.1

7.1 *Appendix 1--Testing Software*

```
1 REM ***THIS IS THE FUNCTION GENERATION PROGRAM TO CONTROL THE FRACTURE TESTS
2 REM ***FOR LOW TEMPERATURE CRACKING OF ASPHALT CONCRETE.***
10 SETDIM N(20,0)
20 C$=F$+"C"
30 OPEN 'DU0:NEW1.DEF' FOR INPUT AS FILE #1 ERROR Z
40 INPUT #1,M1$
50 INPUT #1,M2$
60 INPUT #1,M3$
70 INPUT #1,M4$
80 INPUT #1,M5$
90 INPUT #1,M6$
100 INPUT #1,D1,L1,S1
110 INPUT #1,M7$
120 INPUT #1,M,T,A,A0,A9,E
130 INPUT #1,C1,C2,C3,C5,C6,C7,E1,E2,E3
140 INPUT #1,E4,R8,R9
150 INPUT #1,T2,T1,M2,N,N(1,0),N(2,0),N(3,0),N(4,0)
160 INPUT #1,T3
170 INPUT #1,T4,T5
180 INPUT #1,V5,P4,P5,P6,R5
190 INPUT #1,F$
200 CLOSE
210 CLRTXWIN
220 TXTBOLD \ PRINT '    THIS IS THE FUNCTION GENERATION ROUTINE        '
230 PRINT '    for the THREE-POINT-BEND TEST        ' \ TXTNORMAL
240 PRINT  \ PRINT
245 PRINT 'INPUT FILE NAME' \ INPUT F$
250 SETDIM B((N*2),0)
260 SETDIM VA1(1500,3),VA2(1500,3),VA3(500,3)
270 CLINIT(S)
280 KBINT('A',7, LINE 810 )
290 KBENB
300 CLREMOTESWITCH(1,2,4,0)
310 PRINT 'IS THE STRAIN RANGE';4;'NOW(Y OR N)?' \ INPUT Y1$
320 CKTIME(1,T4)
330 ADTIMED(1,VA1,,1,T5,2,3) \ ADTIMED(3,VA3,,1,T5,15,16)
340 ADTIMED(2,VA2,,1,T5)
350 ADSLAVE(2,15,16)
360 ADIMMED(1,F3)
370 ADIMMED(2,F5)
380 PRINT 'CURRENT SEATING LOAD IS:';ABS(F3)*10;'FROM ADIMMED'
390 PRINT ' INPUT CONTROL LOAD END LEVEL(SHOULD HIGHER THAN:)';ABS(F3)*10;
400 PRINT ' INPUT THIS LOAD ABOUT 4.0*SEATING LOAD';4*ABS(F3)*10;
410 INPUT M4 \ REM*** ONLY FOR SCHIST TEST ****
412 T3=(M4/10-ABS(F3))/T1
414 PRINT 'T3 That will be used in DATAR is:';T3;'SEC'
420 PRINT 'IS THE FILE NAME '; \ TXTBOLD \ PRINT F$; \ TXTNORMAL \ PRINT ' THE CORRECT S
430 IF Q$< >'N' THEN 450
440 PRINT 'THEN INPUT THE CORRECT FILE NAME:'; \ INPUT F$
450 PRINT 'F5=';F5
460 PRINT 'PRESS <CR> TO START' \ INPUT S$
470 ADINIT
480 FOR J=1 TO N
490 B(J,0)=N(J,0)*(T2/1000)
500 NEXT J
510 FOR J=1 TO N
512 SETDIM VA3(500,3),VA4(800,3)
514 ADTIMED(3,VA3,,1,T5,15,16) \ ADTIMED(3,VA4,,1,T5,15,16)
520 Z1=B(J,0)
```

```
530 FGARB(1,"RAMP", RATE T1,Z1)
540 ADGO \ FGGO
550 FGSTATUS(1,K) \ IF K<1 THEN 610
560 ADIMMED(1,F4)
570 ADIMMED(2,F8)
580 IF ABS(F4)>=.985 THEN PRINT 'CURRENT LOAD>=.985 VOLTS' \ GO TO 730
590 IF ABS(F8)>=.985 THEN PRINT 'CURRENT CMOD>=.985 VOLTS' \ GO TO 730
600 IF K>0 THEN 550
610 ADHOLD \ FGSTOP \ FGREMOVE
611 F1$=F$+"C"
612 C$=F1$+STR$(J)
613 OPEN 'DU2:'+C$+'.DAT' FOR OUTPUT AS FILE #4 FILESIZE 60
614 AOUT(4,VA3,,0,Z)
615 CLOSE
616 VADELETE(VA3)
620 S1=.1*F5
630 FGARB(1,"RAMP", RATE T1,S1)
640 ADRESUME \ FGGO
650 FGSTATUS(1,K)
660 IF K<1 THEN 710
670 ADIMMED(1,F9)
680 IF ABS(F9)<=ABS(M4/10) THEN PRINT 'F9=';F9;'M4/10=';M4/10 \ GO TO 700
690 IF K>0 THEN 650
700 ADHOLD \ FGSTOP
701 F2$=F$+"D"
702 D$=F2$+STR$(J)
703 OPEN 'DU2:'+D$+'.DAT' FOR OUTPUT AS FILE #5 FILESIZE 60
704 AOUT(5,VA4,,0,Z)
705 CLOSE
706 VADELETE(VA4)
710 NEXT J
720 ADHOLD \ FGSTOP
730 PRINT 'END OF TESTING'
740 FGARB(1,"RAMP", TIME 2,.4*F5)
750 ADRESUME \ FGGO
760 FGSTATUS(1,K) \ IF K<1 THEN 780
762 ADIMMED(1,Q2)
764 IF ABS(Q2)<=ABS(M4/10) GO TO 780
770 IF K>0 THEN 760
780 ADSTOP \ FGSTOP
790 CLLOCALSWITCH(1)
800 REM**********DATA COLLECTION SYSTEM**********
810 A$=F$+"A" \ B$=F$+"B"
820 OPEN 'DU2:'+A$+'.DAT' FOR OUTPUT AS FILE #3, FILESIZE 65
830 AOUT(3,VA1,,0,Z)
840 CLOSE
850 OPEN 'DU2:'+B$+'.DAT' FOR OUTPUT AS FILE #2, FILESIZE 65
860 AOUT(2,VA2,,0,Z)
870 CLOSE
880 FOR L=0 TO VA1 \ PRINT ELEVEL(VA1(L,1)) \ NEXT L
890 PRINT ' THIS PROGRAM CAN DO FRACTURE TESTING'
892 PRINT ' FOR THE DATA DEDUCTION IF THE TEST IS FOR THE STRAIGHT'
893 PRINT ' LINE NATCH SPECIMEN (ASTM), THEN "QUCK" CAN DO MODULS'
894 PRINT ' AND DIMENSIONLESS COMPLIANCE CALCULATION. "ASTDR2" CAN'
895 PRINT ' GENERATE THE PLOT ON SCREEN OR PLOTTER.'
896 PRINT ' THE PROGRAM STORES DATA OF EACH CYCLE, UNLOADING CYCLE'
897 PRINT ' (D$) AND LOADING CYCLE (C$). ASLO, THE ALL DATA ARE'
898 PRINT ' STORED IN A$,B$. "QUDDU" CAN PLOT DATA EACH CYCLE.'
899 PRINT ' DATA DEDUCTION FOR THE V NATCH (ISRM) IS "DATAR"'
900 PRINT 'TO TRANSFOR DATA TO PC TO PLOT CALL "3PBMDA IN DU0"'
```

```
10 REM *** THIS IS THE DATA DEDUCTION PROGRAM FOR CALCULATING THE KIC
20 REM *** AND DIMENSIONLESS COMPLIANCE (DEB) FOR ASPHALT CONCRETE AT
22 REM *** THE LOW TEMPERATURE ***
30 SETDIM VA5(600,3),VA6(600,3),K(10),S(10),U(10),VA7(600,3)
40 PRINT 'SAMPLE NO.' \ INPUT B
50 PRINT 'MATERIAL:' \ INPUT K$
60 PRINT 'INPUT INITIAL NATCH LENGHT a  (MM)' \ INPUT A
70 PRINT ' INPUT SPECIMEN DEPTH W (MM)' \ INPUT W
80 PRINT 'THE RATIO OF a/w IS ';A/W
90 PRINT 'INPUT POSSION RATIO V ' \ INPUT V
100 PRINT 'INPUT SPECIMEN WIDTH B (MM)' \ INPUT B
110 PRINT 'INPUT F(A/W)'
120 PRINT 'IF A/W = OR NEAR 0.1 THEN INPUT 0.036159'
130 PRINT 'IF A/W = OR NEAR 0.2 THEN INPUT 0.137647'
140 PRINT 'IF A/W = OR NEAR 0.35 THEN INPUT 0.450673'
150 INPUT F1
160 PRINT 'INPUT CYCLES N' \ INPUT N
170 PRINT 'INPUT LVDT CALIBRITION C5' \ INPUT C5
180 PRINT 'INPUT LVDT CALIBRITION C6' \ INPUT C6
190 PRINT 'INPUT FILE NAME' \ INPUT F$
200 PRINT \ PRINT
210 L=8.925*25.4
220 O1=L*L*L/4/B/W/W/W+1.2*L*(1+V)/2/B/W+(L/5/W+5)/B
230 O2=2*L*L*(1-V*V)/B/W/W
240 F1$=F$+"D"
250 FOR J=1 TO N
251 VADELETE(VA5) \ VADELETE(VA6) \ VADELETE(VA7)
252 SETDIM VA5(600,3),VA6(600,3),VA7(600,3)
260 D$=F1$+STR$(J)
270 OPEN 'DU2:'+D$+'.DAT' FOR INPUT AS FILE #1 FILESIZE 60
280 AINP(1,VA5,,0,Z)
290 CLOSE
292 PRINT J,VA5
300 IF J=1 THEN R1=VA5(0,1)
310 IF J=1 THEN R2=VA5(0,2)
320 IF J=1 THEN R3=VA5(0,3)
330 FOR L=0 TO VA5 \ FOR L1=0 TO 3
340 VA6(L,L1)=0 \ VA7(L,L1)=0
350 NEXT L1 \ NEXT L
360 FOR I=0 TO VA5
370 VA6(I,2)=ABS(ELEVEL(VA5(I,2))-ELEVEL(R2))*10*C5*25.4
380 VA6(I,3)=ABS(ELEVEL(VA5(I,3))-ELEVEL(R3))*10*C6*25.4
390 VA6(I,1)=ABS(ELEVEL(VA5(I,1))-ELEVEL(R1))*10*280.94*4.448/1000
400 VA7(I,1)=(VA6(I,2)+VA6(I,3))/2
410 NEXT I
420 REM**** FIND Fmax***
430 P9=0
440 FOR I=0 TO VA5
450 IF ABS(P9)>ABS(VA6(I,1)) THEN 480
460 P9=VA6(I,1)
470 K1=I
480 NEXT I
490 K(J)=P9
500 Q1=.1*K(1) \ Q2=.4*K(1)
510 FOR I=0 TO VA5
520 IF ABS(Q1)<ABS(VA6(I,1)) THEN 540
530 NEXT I
540 T1=I \ Q4=VA6(T1,1) \ Z2=VA7(T1,1)
550 FOR I=0 TO VA5
```

```
560 IF ABS(Q2) < ABS(VA6(I,1)) THEN 580
570 NEXT I
580 T2=I \ Q3=VA6(T2,1) \ Z3=VA7(T2,1)
581 IF J=1 THEN PRINT T1,T2,Q4,Q3
590 FOR I=T1 TO T2
600 Y1=Y1+VA6(I,1)*VA7(I,1)
610 Y2=Y2+VA6(I,1)
620 Y3=Y3+VA7(I,1)
630 Y4=Y4+VA7(I,1)*VA7(I,1)
640 NEXT I
650 N2=T2-T1+1
660 U(J)=(N2*Y4-Y3*Y3)/(N2*Y1-Y2*Y3)
670 PRINT 'MAX LOAD FOR CYCLE';J;'IS';K(J);' AT POINT ';K1
680 P1=.3*K(J) \ P2=.6*K(J)
690 FOR I=K1 TO VA5
700 IF ABS(P1) > ABS(VA6(I,1)) THEN 720
710 NEXT I
720 PRINT 'I=';I;'FOR 0.3*MAX LOAD' \ L1=I
730 P3=VA6(L1,1) \ X3=VA7(L1,1)
740 PRINT 'LOAD IS';P3;'KN';'.  LVDT IS';X3;'MM'
750 FOR I=K1 TO VA5
760 IF ABS(P2) > ABS(VA6(I,1)) THEN 780
770 NEXT I
780 PRINT 'I=';I;' FOR 0.6*MAX LOAD' \ L2=I
790 P4=VA6(L2,1) \ X4=VA7(L2,1)
800 PRINT 'LOAD IS';P4;'KN';'.  LVDT IS';X4;'MM'
810 G1=0 \ G2=0 \ G3=0 \ G4=0
820 FOR I=L2 TO L1
830 G1=G1+VA6(I,1)*VA7(I,1) \ REM** SUM OF X*Y
840 G2=G2+VA6(I,1) \ REM** SUM OF Y
850 G3=G3+VA7(I,1) \ REM** SUM OF X
860 G4=G4+VA7(I,1)*VA7(I,1)
870 NEXT I
880 N1=L1-L2+1
890 S(J)=(N1*G4-G3*G3)/(N1*G1-G2*G3)
900 E=(O2*F1+O1)/U(1)
910 PRINT ' THEN STIFFNESS OF CYCLE';J;' IS ';1/S(J);' KN/MM '
920 PRINT ' THE COMPLIANCE OF CYCLE';J;' IS ';S(J);' MM/KN'
930 PRINT 'THEN E =';(O2*F1+O1)/U(1);' KN/(MM**2)'
940 PRINT 'DEMINTIONLESS COMPLIANCE(CEB)=';S(J)*E*B;' FOR CYCL ';J
950 PRINT  \ PRINT
960 NEXT J
970 END

Ready
```

```
20 REM ** THIS PROGRAM IS TO GRAPHIC FUNCTION. IT CAN PLOT THE TEST DATA
30 REM *** ON THE SCREEN OR ON THE PLOTTER FOR THE ASPHALT CONCRETE TEST
40 REM *** AT THE LOW TEMPERATURE.
50 OPEN 'DU0:ASTEST.DAT' FOR INPUT AS FILE #1 ERROR Z
60 INPUT #1,M1$
70 INPUT #1,M2$
80 INPUT #1,M3$
90 INPUT #1,M4$
100 INPUT #1,M5$
110 INPUT #1,M6$
120 INPUT #1,W,L,S
130 INPUT #1,M7$
140 INPUT #1,A,E,T2,T3,T4,T5
150 INPUT #1,C1,C2,C3,C5,C6,C7,E1,E2,E3,E4
160 INPUT #1,T1,M2,N
170 CLOSE
180 DIM VA1(1500,3),VA2(1500,3)
185 PRINT 'INPUT FILE NAME' \ INPUT F$
186 PRINT ' INPUT SAMPLE NO.' \ INPUT M3$
187 PRINT ' INPUT MATERIAL DESCRIBTION ' \ INPUT M6$
190 A$=F$+'A' \ B$=F$+'B'
200 OPEN 'DU2:'+A$+'.DAT' FOR INPUT AS FILE #1 FILESIZE 65
210 AINP(1,VA1,,0,Z)
220 CLOSE
230 OPEN 'DU2:'+B$+'.DAT' FOR INPUT AS FILE #2 FILESIZE 65
240 AINP(2,VA2,,0,Z)
250 CLOSE
260 SETDIM VA5(1500,3),VA6(1500,3),VA7(1500,3)
270 PRINT \ PRINT 'INPUT CURRENT SPECIMEN TEMPERATURE T' \ INPUT T
272 PRINT 'INPUT NATCH LENGTH a' \ INPUT A
274 PRINT 'INPUT SPECIMEN WIDTH w' \ INPUT W
280 FOR I=0 TO VA1
290 VA5(I,2)=ABS(ELEVEL(VA2(I,2))-ELEVEL(VA2(0,2)))*10*3.99200E-03*25.4
300 VA5(I,3)=ABS(ELEVEL(VA2(I,3))-ELEVEL(VA2(0,3)))*10*4.08280E-03*25.4
310 VA5(I,1)=ABS(ELEVEL(VA2(I,1))-ELEVEL(VA2(0,1)))*10*280.94*4.448/1000
320 VA6(I,1)=ABS(ELEVEL(VA1(I,2))-ELEVEL(VA1(0,2)))*10*.267
330 NEXT I
340 REM*** FIND Fmax **********************
350 LET P9=0
360 FOR I=0 TO VA1
370 IF ABS(P9) > ABS(VA5(I,1)) THEN 390
380 P9=VA5(I,1)
390 NEXT I
400 PRINT 'MAX LOAD IS:';P9;'KN'
410 FOR I=0 TO VA1
420 VA7(I,1)=VA5(I,1)
430 VA7(I,2)=(VA5(I,3)+VA5(I,2))/2
440 VA7(I,3)=VA6(I,1) \ REM*** CMOD
450 NEXT I
460 REM**** PLOT GRAGHIC ***********
470 PRINT 'ENTER 1 FOR SCREEN OR 2 FOR PLOTTER ' \ INPUT G1
472 A1=.07 \ A2=7.00000E-03
474 B1=2.3 \ B2=.23
480 IF G1=1 THEN 750
490 IF G1=2 THEN Z5=1
500 GRATTACH(G1,2) \ GRON(G1) \ COLORLINE(G1,1)
510 PHYL(G1,5,65,5,85)
520 SCALE(G1,0,0,A1,0,B1)
530 LABEL(G1,'LOAD POINT DIS. mm','LOAD KN',A2,B2,0)
```

```
540 INVEC(G1)
545 PLOT(G1,0,B1)
550 IF G1=2 THEN COLORLINE(2,2)
560 FOR I=0 TO VA1
570 PLOT(G1,VA7(I,2),VA7(I,1))
580 NEXT I
590 PHYL(G1,65,100,0,100)
600 SCALE(G1,0,0,80,0,80)
610 F2$='Fmax='+(STR$(P9))+'KN'
620 COMM(G1,F2$,10,60)
630 H$='a/w='+(STR$(A/W))
640 T$='TEMP:'+(STR$(T))+'DEG.C'
650 S$='No.'+M3$
660 R$='MATERIAL:'+M6$
680 COMM(G1,H$,5,20)
690 COMM(G1,S$,5,50)
700 COMM(G1,T$,5,40)
710 COMM(G1,R$,5,30)
720 PRINT 'COPY GRAPH TO PLOTTER (Y OR N)?' \ INPUT Q2$
730 IF Q2$< >'Y' THEN 770
740 G1=2 \ GO TO 500
750 ERASE(1)
760 TEKMODE(1,1) \ TEKON(1) \ GO TO 510
770 TEKOFF(1)
780 END

Ready
```

7.2 *Appendix 2--Fracture Tests*

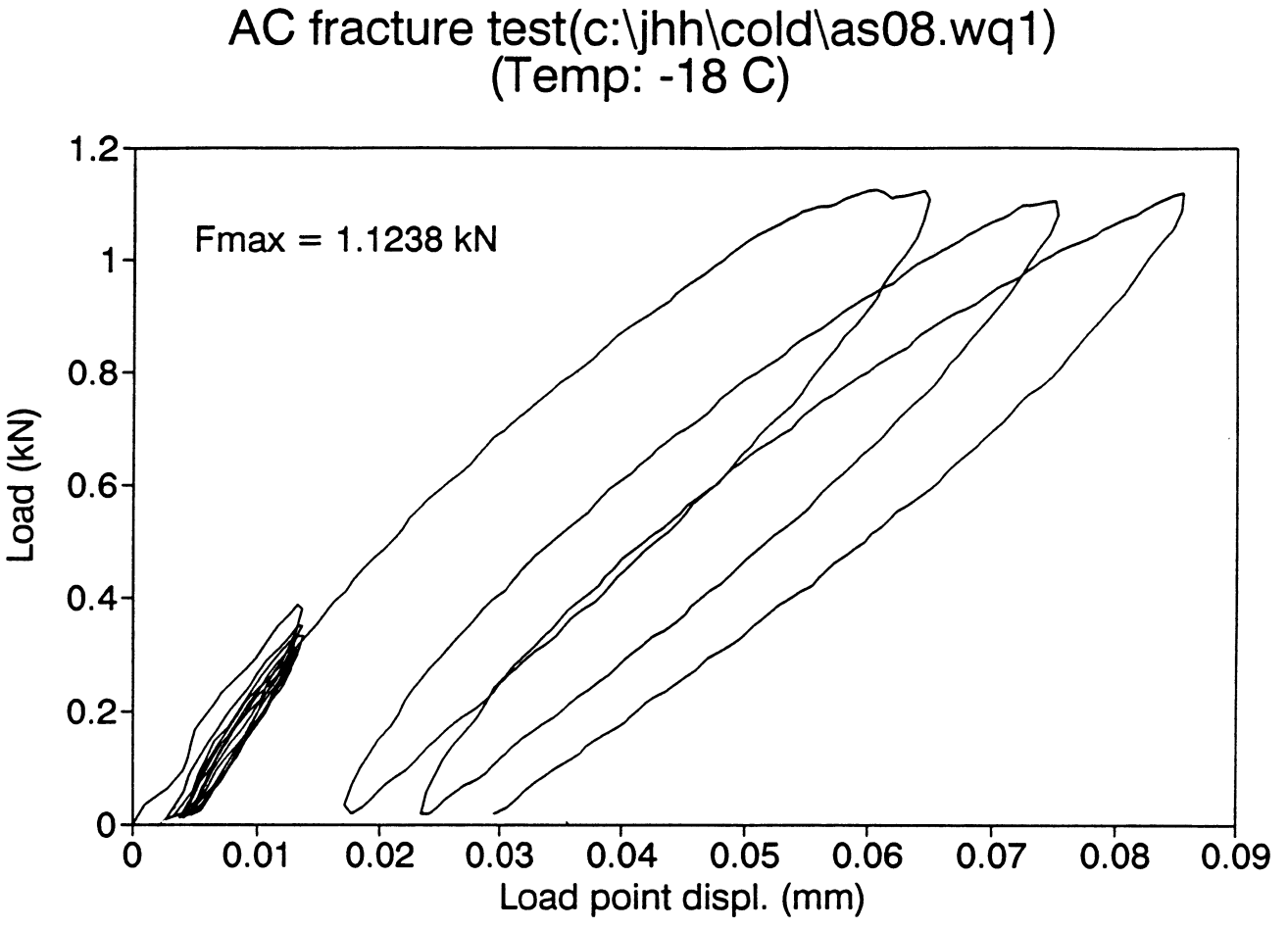
AC fracture test(c:\jhh\cold\as08.wq1)
(Temp: -18 C)
Fmax = 1.1238 kN
Load (kN)
1.2
1
0.8
0.6
0.4
0.2
0
0
0.01
0.02
0.03
0.04
0.05
0.06
0.07
0.08
0.09
Load point displ. (mm)

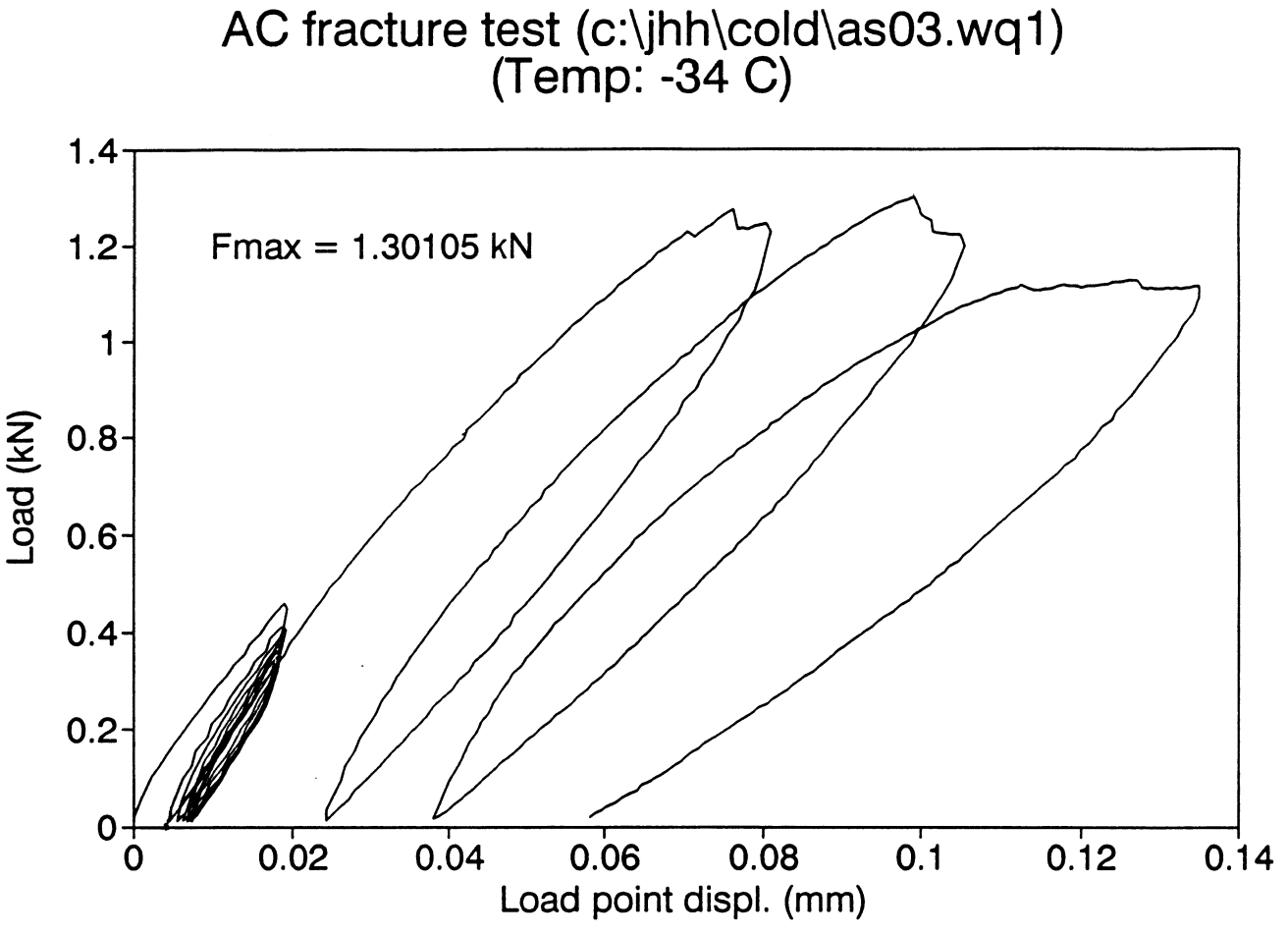
AC fracture test (c:\jhh\cold\as03.wq1)
(Temp: -34 C)
Fmax = 1.30105 kN
Load (kN)
1.4
1.2
1
0.8
0.6
0.4
0.2
0
0
0.02
0.04
0.06
0.08
0.1
0.12
0.14
Load point displ. (mm)

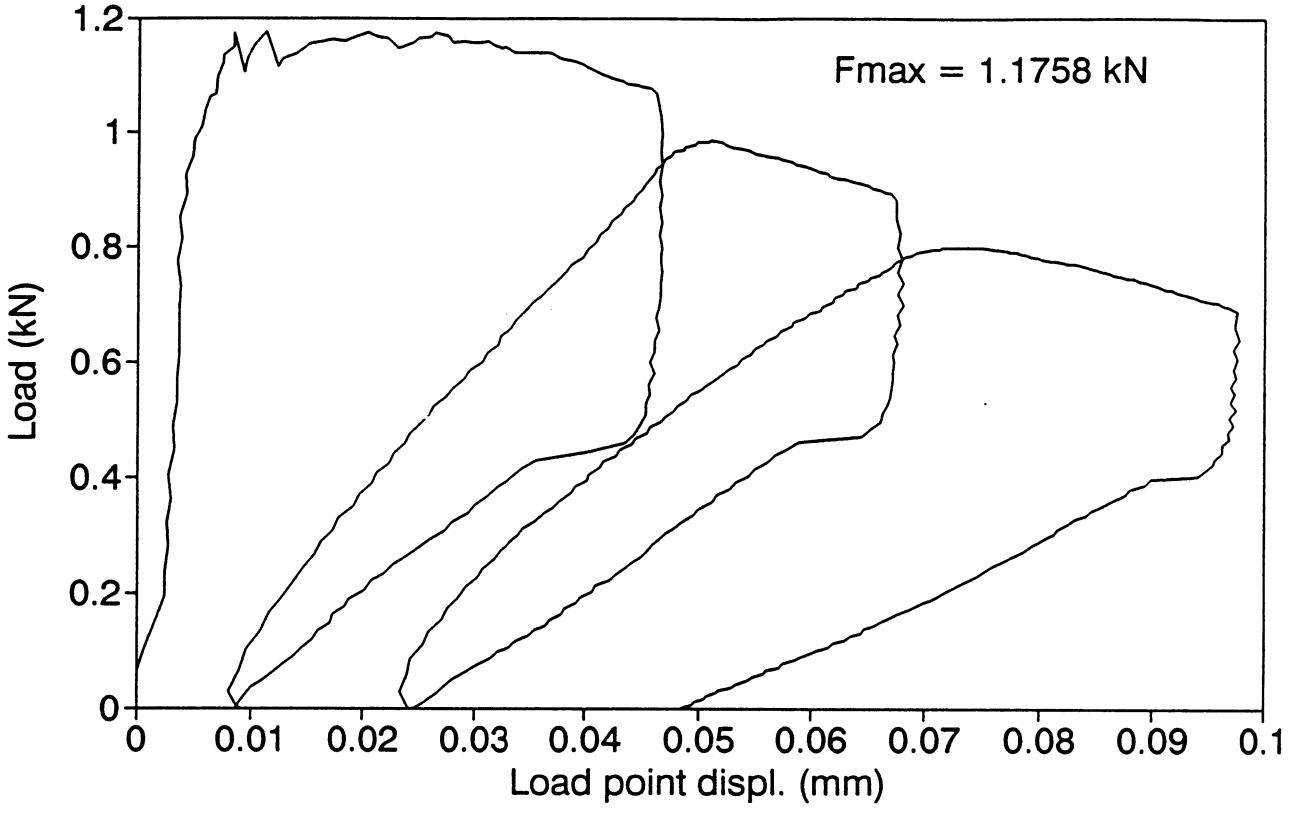
AC fracture test(c:\jhh\cold\as09.wq1)
(Temp: -34 C)
Fmax = 1.1758 kN
Load (kN)
1.2
1
0.8
0.6
0.4
0.2
0
0
0.01
0.02
0.03
0.04
0.05
0.06
0.07
0.08
0.09
0.1
Load point displ. (mm)

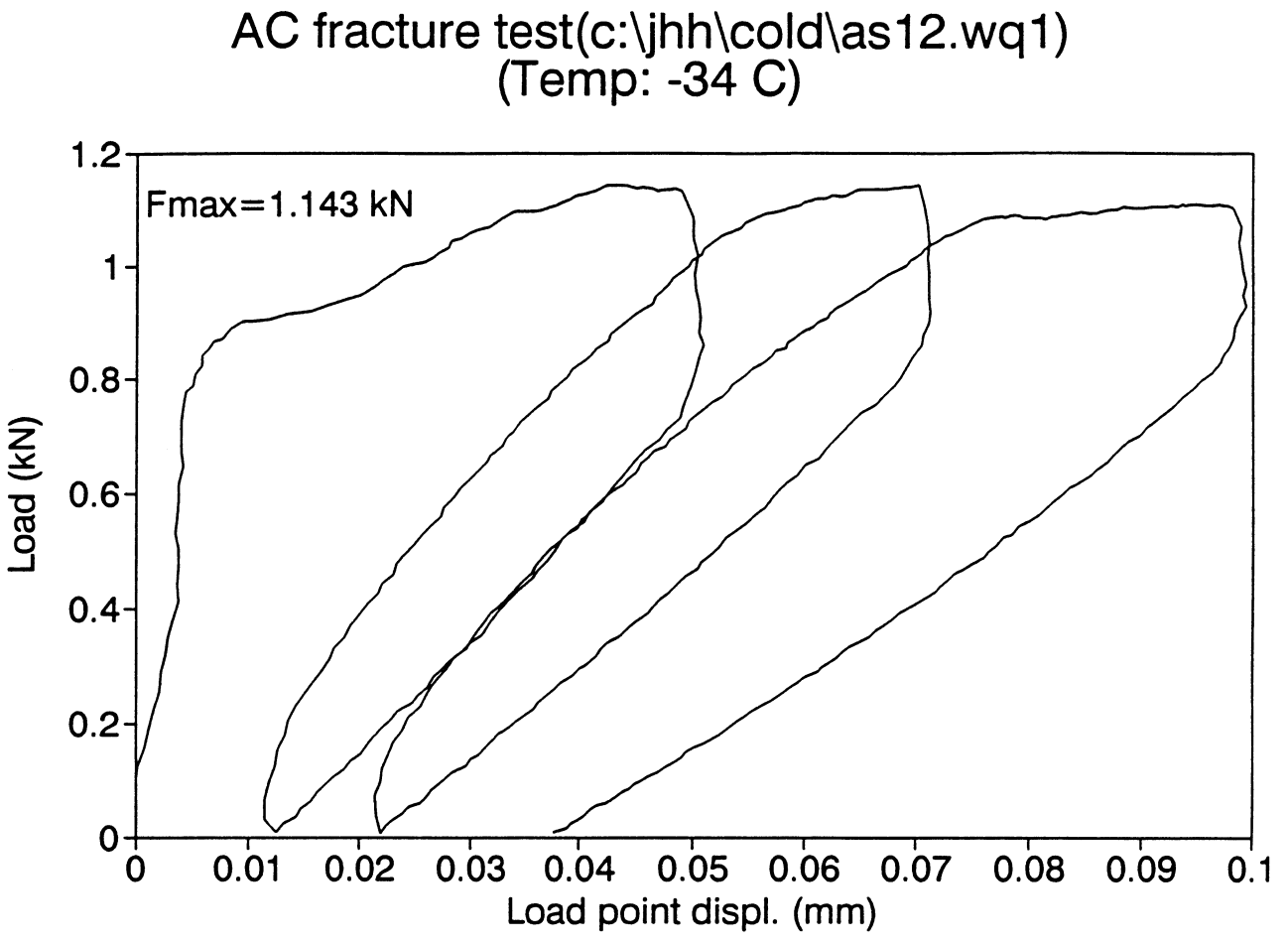
AC fracture test(c:\jhh\cold\as12.wq1)
(Temp: -34 C)
Fmax=1.143 kN
Load (kN)
1.2
1
0.8
0.6
0.4
0.2
0
0
0.01
0.02
0.03
0.04
0.05
0.06
0.07
0.08
0.09
0.1
Load point displ. (mm)